Generated using the official AMS LaTeX template v5.0

Future Projections of Heat Mortality Risk for Major European Cities

Alexia Karwat[1,2] and Christian L. E. Franzke[3,4,5,6*]

[1]*Institute for Meteorology and Climatology, Leibniz University of Hannover, Hannover, Germany*

[2]*Meteorological Institute, University of Hamburg, Hamburg, Germany*

[3]*Center for Earth System Research and Sustainability, University of Hamburg, Hamburg, Germany*

[4]*School of Engineering and Science, Jacobs University, Bremen, Germany*

[5]*Center for Climate Physics, Institute for Basic Science (IBS), Busan, Republic of Korea*

[6]*Pusan National University, Busan, Republic of Korea*

DRAFT

[*]*Corresponding author*: Christian L. E. Franzke, christian.franzke@gmail.com

ABSTRACT

Over the last few decades heat waves have intensified and have led to excess mortality. While the probability of being affected by heat stress has significantly increased, the risk of heat mortality is rarely quantified. This quantification of heat mortality risk is necessary for systematic adaptation measures. Furthermore, heat mortality records are sparse and short, which presents a challenge for assessing heat mortality risk for future climate projections. It is therefore crucial to derive indicators for a systematic heat mortality risk assessment. Here, risk indicators based on temperature and mortality data are developed and applied to major cities in Germany, France and Spain, using regional climate model simulations. Bias-corrected daily maximum, minimum and wet-bulb temperatures show increasing trends in future climate projections for most considered cities. Additionally, we derive a relationship between daily maximum temperatures and mortality for producing future projections of heat mortality risk due to extreme temperatures based on low (Representative Concentration Pathway; RCP2.6) and high (RCP8.5) emission scenario future climate projections. Our results illustrate that heat mortality increases by about 0.9%/decade in Germany, 1.7%/decade in France and 7.9%/decade in Spain for RCP8.5 by 2050. The future climate projections also show that wet-bulb temperatures above $30°C$ will be reached regularly with maxima above $40°C$ likely by 2050. Our results suggest a significant increase of heat mortality in the future, especially in Spain. On average, our results indicate that the mortality risk trend is almost twice as high in all three countries for the RCP8.5 scenario compared to RCP2.6.

DRAFT

Significance statement. Human made greenhouse gas emissions have led to an increase in temperatures over the last century. This general warming leads to more intensive and more frequent heat waves which affect humans adversely. Extreme temperatures exert heat stress on the human body and can lead to reduced productivity, sickness and death. Here we derive a statistical relationship between extreme temperatures and the number of deaths in major cities in three European countries in order to be able to use future climate simulations to determine likely numbers of heat related deaths. Our results show that the number of heat related deaths will increase in major European cities by 2050 and will be twice as high for high compared to low greenhouse gas emissions simulations.

1. Introduction

Thousands of people die every year in Europe due to exposure to extreme heat (Merte 2017; Franzke and Torello i Sentelles 2020). For example, high temperatures associated with the 2018 or 2019 heat waves tend to become the new normal (Mitchell et al. 2019). Only the heat wave of 2003 has been warmer; 2003 was actually the warmest in over 500 years (Luterbacher et al. 2004), and caused approximately 30.000-70.000 fatalities in Europe, almost half of them in France (Poumadère et al. 2005; Robine et al. 2008). Heat stress was also severe in Germany in 2006, 2010, 2013, 2015 and 2019 with more than 10 days considered as hot days where temperatures reached more than $30°C$ (Umweltbundesamt 2019). A general increase in the intensity and frequency of extreme events has also been reported for Spain (Ecologistas en Acción 2019) as well as

DRAFT

increases of human health risks worldwide (Smith et al. 2014). These observed changes are due to anthropogenic global warming (Seneviratne et al. 2012).

Climatic risks are not only defined by climate extremes but also by the vulnerability of a society and its exposure to natural hazards (Masson-Delmotte et al. 2018). A high-level risk for the current and future health of global populations is discussed in various reports of the medical journal The Lancet (Gasparrini et al. 2017; Watts et al. 2018, 2019, 2021). Due to the increasing frequency of heat waves, there has been a considerable increase in the risks of heat stress, and cardiovascular, respiratory and renal diseases. These diseases put populations in Europe at particular risk as about 42% of their population is older than 65 years (Watts et al. 2018); elderly people are more vulnerable to heat stress (Robine et al. 2008). Furthermore, heat mortality vulnerability is estimated to be 15% - 22% higher in the largest European cities for a $2°C$ compared to a $1.5°C$ warming (Orlov et al. 2019) and could be significantly reduced if global warming is stabilized below $1.5°C$ (Masson-Delmotte et al. 2018; Wang et al. 2019). It is likely that anthropogenic climate change will increase the heat mortality risk potential (Franzke 2017; Franzke and Torello i Sentelles 2020).

There are several case studies on European cities (Ishigami et al. 2008; Todd and Valleron 2015) or selected European countries in, for example, Gasparrini et al. (2015); Kendrovski et al. (2017), which focus on heat and mortality. Higher mortality risk from heat waves that are more intense or longer is also a current issue investigated in i.e. Anderson and Bell (2011).

DRAFT

Heat stress is caused by the combination of temperature and humidity, which can efficiently be quantified by the wet-bulb temperature (Sherwood and Huber 2010; Coffel et al. 2017; Pal and Eltahir 2016; Kang and Eltahir 2018; Im et al. 2017), though this is a simplification which neglects other important quantities such as wind speed and radiant temperature (Havenith 2005). The wet-bulb temperature is one common method amongst other approaches, for example, the apparent temperature or the "Klima-Michel-Modell" of the German Weather Service (Jendritzky et al. 1990; Matzarakis et al. 2020).

Humidity is an important physiological variable for human health due to its universal impact on air quality, respiratory diseases, influenza, heat stress and mortality (Davis et al. 2016) and defined by, for example, wind speed and radiant temperature (Havenith 2005). Humidity has also been associated as a direct link between hot weather extremes, mental health issues and illnesses (Ding et al. 2016). As heat stress is estimated to intensify considerably in the decades to come, the potential of a wide spread exposure to deadly wet-bulb temperatures approaching or exceeding the theoretical limit of human tolerance is an important part of current research (Pal and Eltahir 2016; Kang and Eltahir 2018; Im et al. 2017). During the deadly 2003 European and 2010 Russian heat waves, wet-bulb temperatures reached between 23°C and 31°C (Raymond et al. 2020; Coffel et al. 2017). Furthermore, future climate projections indicate that certain regions will be regularly affected by deadly heat waves in high emission scenarios by the end of this century (Pal and Eltahir 2016; Kang and Eltahir 2018; Im et al. 2017). Extreme wet-bulb temperatures of 35°C can be prevented in the tropics when limiting global warming to

DRAFT

1.5°C (Zhang et al. 2019), while current wet-bulb temperatures of 31°C and higher are rare in European climate and would remain so without anthropogenic global warming (Coffel et al. 2017). A study of the threshold between lethal and non-lethal heat episodes found that wet-bulb temperatures above 37°C cause hyperthermia (Mora et al. 2017). Here we will examine how often such heat stress thresholds will be crossed in future climate projections.

A trend analysis of climate risk is typically based on climate extreme indices i.e. temperature thresholds or return periods. Traditionally, linear regression is used, however, due to the large variability of temperature extremes, results are often not robust. Using quantile regression, which estimates changes over time of certain percentiles of temperature, changes in extremes can be detected more clearly (Gao and Franzke 2017). There have also been attempts to define a minimum mortality temperature (Yin et al. 2019), to introduce a climate-damage function (Dell et al. 2014), and to establish climate risk indices (Bündnis Entwicklung Hilft 2019; GermanWatch 2019a,b; Society of Actuaries 2019). A few also focused on building disaster databases (Centre for Research on the Epidemiology of Disasters (CRED) 2019), interactive risk explorers (Karlsruher Institut für Technologie (KIT) 2019; UNEP/GRID-Geneva 2019) or publishing climate signal maps (Climate Service Center Germany (GERICS) 2019). A location-specific heat wave vulnerability index has been established for London (Wolf and McGregor 2013). Recent research also focuses on more intuitive ways to communicate the societal impacts of extreme temperature risks. An example is a statistical approach to quantify the similarity of a city's climate to the climate of another location by investigating the climatic

DRAFT

analogs of more than 500 North American urban areas (Fitzpatrick and Dunn 2019). Urban areas from the Northern Hemisphere are shifting towards warmer conditions; for instance, London's climate in 2050 will resemble Barcelona's climate today, Madrid's future climate will be more similar to Marrakesh's current climate (Bastin et al. 2019). However, this climatic similarity does not tell us much about how these cities will deal with the effects of warming and how they will affect mortality; while Barcelona has the infrastructure to deal with extreme temperatures, London might not. Thus, systematic heat mortality risk assessments are also needed for adaptation planning. Thus, the observed relationship between extreme temperatures and heat mortality in urban areas also needs to be quantified.

The aim of this study is to systematically quantify heat stress and mortality risk in 48 cities in Germany, France and Spain. Thereby, our analysis is threefold:

1. We investigate trends in daily maximum (TX) and minimum (TN) temperatures during the period 1950-2018 and use them to evaluate the output from regional climate models to predict heat stress under different greenhouse gas emission scenarios.

2. We further investigate heat stress through an analysis of an empirically modeled wet-bulb temperature, which we examine in historical climate simulations and future climate projections.

3. We also project excess heat deaths in RCP2.6 and RCP8.5 until 2050 by combining observations of TX and mortality using a regression model.

DRAFT

In contrast to most previous studies on heat mortality we focus on long-term trends; most previous studies used rather short observational time series (Carleton et al. 2020).

As a consequence, this study is organized as follows. In section 2, we introduce the data and the study area. Subsequently, the statistical methods are presented, whereby heat stress and mortality risk indicators are defined. In section 3, results from the analysis will be discussed. Conclusions will be presented in section 4.

2. Data and Methods

In this study, we use daily gridded observations obtained from the observation-based data set E-OBS (Cornes et al. 2018) version 19.0e (Copernicus Climate Change Service (C3S) 2019). The data set is based on daily meteorological station data from January 1950 through December 2018 on a 0.1 degree regular grid, covering Europe from 25.0°N to 71.5°N and 25.0°W to 45.0°E. We focus on the summer months June through August (JJA).

Regional future climate projections originate from combinations of global and regional climate models and include historical runs and future climate projections based on greenhouse gas emission scenarios RCP2.6 and RCP8.5 until 2050 from the EURO-CORDEX initiative (2019). We use data from the regional climate models CCLM (Cosmo Climate version of Local Model) and RACMO driven by the global climate model EC-EARTH, REMO2009 driven by MPI-ESM-LR and REMO2015 driven by NorESM1-M. The climate model data include maximum and minimum temperatures and relative humidity, which are used to calculate the wet-bulb temperature. A summary

DRAFT

of the available data of maximum (TX) and minimum temperature (TN), and relative humidity (RH) is given in Tab. 1. All data is interpolated onto the same regular grid as the E-OBS data with a resolution of 0.1 degree. TX and TN are bias-corrected as shown in section 1, while humidity data are not adjusted to the bias-corrected air temperatures because E-OBS does not provide humidity data. The RCM data is interpolated to the same grid as the E-OBS data.

a. Wet-bulb temperature

Since the wet-bulb temperature TW is an important proxy for the ability of the human body to endure heat, we use it to assess climate impacts on health under extreme conditions, for example, during long-lasting heat waves. The composite effect of temperature, in this case TX or TN, and relative humidity is a significant factor of climate risk. Essentially, the wet-bulb temperature relates to human comfort as much as it relates to human health. The higher the wet-bulb temperature, the higher the discomfort, and the higher the risk of the human's body to succumb to heat death (Coffel et al. 2017).

We compute the wet-bulb temperature as defined by Stull (2011). Stull (2011) created an empirical formula for the wet-bulb temperature using gene-expression programming (GEP). This algorithm learns specifically about relationships between variables and then builds models to explain these relationships. GEP can find a best fit of the function and yield a nonlinear result like Equation (1). In Equation (1) the temperatures are in degrees celsius and the relative humidity in percent. The input data for this regression are for standard sea level pressure of 101.325 kPa. Pressure was not used as one of the

DRAFT

predictor variables so that the resulting regression does not vary with pressure. Equation (1) refers to an arc-tangent function, with T as the maximum or minimum temperature in $^{\circ}C$, while relative humidity is applied in %:

$$T_w = T\,\mathrm{atan}[0.151977(\mathrm{RH\%}+8.313659)^{1/2}] + \mathrm{atan}(T+\mathrm{RH\%}) - \mathrm{atan}(\mathrm{RH\%}-1.676331) + 0.00391838(\mathrm{RH\%})^{3/2}\mathrm{atan}(0.023101\mathrm{RH\%}) - 4.686035. \quad (1)$$

b. Study Area

To illustrate the study area and the cities included in the trend analysis, the selected points of interest are presented in Fig. 1 and Tab. 2. The methods applied to the cities depend on the original grid type of each climate model and the standard grid size of 3 x 3 grid points, corresponding to 0.3 x 0.3 degrees on the E-OBS grid. Generally, this is the most fitting grid size as applying a larger grid-box with 4 x 4 or 5 x 5 grid points would entail suburban areas that do not lie within the main range of interest of most cities.

In many statistical temperature analyses the urban heat island effect (Kalnay and Cai 2003) is removed, since it is not a direct climate effect. However, since we are here interested in the direct effect of heat on humans, we do not need to remove the urban heat island effect. This effect actually contributes to the heat stress of humans in urban areas. However, most climate models do not account for urban surfaces due to cities representing only a very small subset of the full resolution data set (Oleson et al. 2011); this will likely underestimate the extreme temperatures in urban areas in our study.

DRAFT

c. Data Analysis

1) Bias-correction of regional climate models

Due to their limited spatial resolution, regional climate models often show systematic biases that are the result of unresolved scales and physical processes, parameterization from simplified physics and thermodynamic processes or incomplete knowledge of climate system processes (Stensrud 2009). It is therefore necessary to bias-correct the raw climate model outputs in order to reduce their systematic biases for future climate projections. There are several methods for bias-correction, for example, quantile mapping (e.g. Maraun 2016). Quantile mapping is often used in climate change impact studies to analyse data with a high variability, for example, precipitation. Previous studies have shown that quantile mapping alternates the magnitude and even the direction of mean changes projected from the original climate model (e.g. Hagemann et al. 2011, Pierce et al. 2013, Maurer and Pierce 2014). This can lead to inconsistent results between the bias-corrected and the original model output. If a climate model has too much variability, quantile mapping tends to reduce variability on all time scales, including the trend. Equally, if the climate model shows too little variability, quantile mapping tends to increase the trend.

Another widely used approach corrects the raw model output using the differences in the mean and of the variability between climate model and observations in a reference period (The CGIAR Research Program on Climate Change, Agriculture and Food Security (CCAFS) 2014; Maraun 2016). More precisely, this approach is called the delta change method and uses daily mean observations ($\overline{obs}$) of the variable from 1950 to

DRAFT

2005, while considering the raw output of the climate model (mod_{raw}) and the mean of the climate model ($\overline{mod}$). Using the delta change method is more suitable in that regard that the linear spatial and temporal structure of the data, i.e. temperature, is preserved. We use a correction coefficient (σ) as a scale parameter to deal with the bias between observations and regional climate model data. This is a common approach as shown in, for example, Hawkins et al. (2013). The correction coefficient is estimated by the difference in the standard deviation of the daily RCM output and of the observations from the three capital cities, which serve as sample sites to adjust the bias in the reference period for all cities. Therefore, the correction coefficient is summarised as:

$$\sigma = \sigma(\overline{obs}) - \sigma(\overline{RCM}) \tag{2}$$

In our study the correction coefficient σ is about 0.2. Hence, we bias correct a temperature T_{BC} from historical climate model data as summarized by:

$$T_{BC} = \overline{obs} + \sigma(mod_{raw} - \overline{mod}) \tag{3}$$

We bias correct future climate projections by subtracting the mean of the RCP scenarios until 2050 ($\overline{mod}$) along with the daily mean observations ($\overline{obs}$) from the past climate reference period (1950-1995) from the daily raw model outputs of 2005-2050 (mod_{raw}). Hence a future time series is generated, which deals with the mean bias. The approach for a bias-corrected temperature projection T_p is therefore defined as follows:

$$T_p = mod_{raw} - (\overline{mod} - \overline{obs}) \tag{4}$$

DRAFT

2) Statistical analysis

In order to identify trends we use quantile regression (Chatterjee and Hadi 2000; Koenker and Hallock 2001) with a linear model and the non-parametric Mann-Kendall test (Mann 1945; Kendall 1975). While standard linear regression represents the change in the mean, quantile regression is able to represent changes in percentiles, and thus can also identify changes in extremes when defined as high percentiles (Donner et al. 2012; Franzke 2015; Gao and Franzke 2017).

Climate time series are autocorrelated and this autocorrelation impedes the identification of trends (Fatichi et al. 2009; Franzke 2012; Franzke et al. 2020). To account for this autocorrelation we use the modified Mann-Kendall trend test by Hamed and Rao (1998). The Mann-Kendall trend test is a non-parametric test for monotonic trends. We use a significance level of 5%. The Mann-Kendall trend test is a commonly used method in the analysis of annual summer temperature trends as shown, for example, by Gavrilov et al. (2018).

d. Human health and heat risk assessment

We use monthly mortality data that is available for selected European cities on a nation-wide scale to relate temperature parameters to mortality risk. Consequently, mortality rates are recorded by the statistical government agencies in Germany (Statistisches Bundesamt Deutschland 2019) `https://www.destatis.de/DE/Themen/Gesellschaft-Umwelt/Bevoelkerung/Sterbefaelle-Lebenserwartung/Tabellen/sonderauswertung-sterbefaelle.html`, France (Institut Na-

DRAFT

tional de la Statistique et des Études Économiques, Paris, France 2019) https://www.insee.fr/fr/statistiques/serie/000436394#Tableau and Spain (Instituto Nacional de Estadística, España 2019) https://www.ine.es/dynt3/inebase/es/index.htm?padre=1132&capsel=1134.

To establish a heat mortality risk indicator we use the following approach. As frequency and recurrence of extreme temperatures are proxy indicators of thermal stress, the level when TX or TN have crossed a critical threshold is a useful method to measure risk. Quantiles are applied to give an overview of the distribution of TX and TN in the specific climate reference period, and particularly, to provide the probability of extreme values. Extreme values of quantiles are defined as measurements of position in space and indicate where a specified proportion of the data distribution can be found (Coles 2001). To establish the risk by specific levels, data of the 50th, 80th, 90th, and 95th percentiles are analyzed for the presence of trends. From the relation between percentiles of temperature with time, the quantile regression is therefore summarised by:

$$model = intercept + slope \cdot T_{percentile} \tag{5}$$

The coefficients from this regression are summarised for the capital cities in Tab. 4 and 5. The regression fit provides statistically significant slopes at the 1% level for all capital cities. Though the R^2-values are rather low, the regressions are still good by capturing the long term behavior as can be seen in Fig. 3. The F-statistics are relatively larger than 1 for all capital cities, given the size of our data.

DRAFT

In addition to TX and TN, the wet-bulb temperature TW is a significant parameter to define climate risk in relation to heat stress, illness and death. TW can be further classified by different warning levels, e.g. DTN (2017). There is evidence that most physical labor becomes unsafe at TW values above $32°C$ as a person would eventually suffer heat illness in the absence of artificial cooling. The theoretical limit of human survival for more than a few hours in the shade is when TW exceeds the level of $35°C$ (Coffel et al. 2017; Sherwood and Huber 2010). Previous studies have considered this as the limit of human tolerance to heat stress. Under long-lasting heat waves with high TW values, the human body's evaporative cooling becomes considerably less effective as the body's heat regulation shuts down completely after about 6 hours under such thermal stress (Kopp et al. 2015; Sherwood and Huber 2010).

Heat mortality is computed by performing linear regression on mean TX values (JJA 1950-2018) and deaths per month in 1990-2018 (Germany) and 1950-2018 (France, Spain), similar to Dushoff et al. (2006). From the relation between deaths per months and mean TX values, the heat mortality linear regression is therefore summarised by:

$$model = intercept + slope \cdot TX_{mean} \tag{6}$$

For Germany, the missing years (1950-1989) are reconstructed using the linear relationship between monthly deaths and mean TX. Deaths are normalized per 100.000 inhabitants for all cities. Furthermore, we assume a constant population size in time of the respective cities and countries for our mortality projections. This assumption makes a comparison with current mortality data easier and also focuses solely on the effect of

DRAFT

heat stress on mortality in the future climate projections. The coefficients from the heat mortality regression are summarised in Tab. 6 for the 68 observations (1950-2018). The regression fit provides statistically significant slopes (p-value $< 2.23 \cdot 10^{-6}$ for Germany, $< 2.51 \cdot 10^{-5}$ for France and $< 3.73 \cdot 10^{-11}$ for Spain) and gives R^2-values of about 0.2 (Germany, France) and 0.4 (Spain). Though the R^2-values are rather low, the regressions are still good by capturing the long term behavior as can be seen in Fig. 2. The rather low R^2-values are due to the relative large spread around the regression line. The F-statistic is 26.81 (Germany), 20.49 (France) and 62.31 (Spain), which is relatively larger than 1 given the size of our data.

We used a dummy variable for different thresholds if the maximum temperature exceeds $33°C$, $35°C$ or $37°C$. However, the p-values are slightly higher for all considered cities and generally, the regression seems not to be influenced by the interaction term of the dummy variable.

Furthermore, we also introduced an additional term to our heat mortality regression that interacts with the regression. The interaction term is defined by the 95th percentile of TX. Therefore, the model is summarised by:

$$model = intercept + slope \cdot TX_{mean} + slope \cdot TX_{95th_{percentile}} \tag{7}$$

Looking at the statistical coefficients, there are no significant differences between R-values from the regression of the capital cities (see Tab. 7 in *Supplementary Material*). The slightly higher p-values suggest less significant slopes; the t-values and F-statistics show even lower values.

DRAFT

We tested our regressions also against World Health Organization (WHO) heat deaths (X30) for the period 2015-2018. Heat deaths are explicitly only recorded since 2015, so we cannot use them in our study on the long-term behavior of heat mortality. Our regression model shows reasonably good skill in hindcasting X30. The projections in 2019-2050 are computed by using the regression coefficients from 1950-2018 under two greenhouse gas emission scenarios: low (RCP2.6) and high (RCP8.5). To carry out the statistical analysis we first compute seasonal summer means for JJA. Then we compute the specified percentiles. Based on these percentile time series we perform the trend tests.

3. Results

First we present the evaluation of TX and TN in E-OBS and RCMs, before we show the wet-bulb temperature (TW) and heat mortality projections. For illustrative purposes, we first focus on the three capital cities before we also discuss the other considered cities.

a. Evaluation of TX and TN observations in E-OBS

In Fig. 3 we display the TX and TN quantile regression trends from daily observations for Berlin, Paris and Madrid for the period 1950-2018 in E-OBS. There is an increase of approximately $3°C$ in the 90th percentile of TX in Berlin. A trend towards more frequent years in which the 90th percentile approaches $30°C$ or more is observed in Paris since the 1990s. The median is characterized by a tendency towards $25°C$ due to a general increase in the maximum temperature. In Madrid, the median is marked

DRAFT

by an increase of 3.4°C from 1950 to 2018. The other percentiles experience trends with slightly lesser increases of approximately 3°C. These trends are consistent with previous studies (Franzke 2015; Haug et al. 2020) and show the marked temperature increase over the last few decades, which is much larger than the global mean surface temperature increase.

As for TN, the 95th percentile is approaching the 20°C level in Berlin more frequently since the late 1970s. In contrast to the median, all other selected percentiles have statistically significantly increased by at least 2.6°C in Paris. Similar to Berlin, the 20°C level is therefore reached more often by upper percentiles. Madrid is marked by an increase between 2.5°C and 2.7°C concerning all selected percentiles. Furthermore, a trend is observed towards TN exceeding 22°C more frequently since the 1990s. Since TN values are indicative of night time temperatures, this suggests that tropical nights have statistically significantly increased over the last few decades. This also contributes to heat stress, because the human body is less able to relax during the night if night time temperatures are above 20°C (Murage et al. 2017).

Overall, there is a tendency visible that the higher percentiles increase faster than the median in the capital cities Berlin and Paris for TX and TN as well as in Madrid for TN. The 95th percentile increases by 0.42°C (TX) and 0.25°C (TN) per decade in Berlin and by 0.55°C (TX) and 0.39°C (TN) per decade in Paris. The median is marked by an increase of about 0.33°C (TX) and 0.21°C (TN) in Berlin and by 0.47°C (TX) and 0.33°C (TN) per decade in Paris. In Madrid, the higher percentiles increase faster only in TN: by approximately 0.4°C/decade in the 95th percentile and by 0.37°C/decade in

DRAFT

the median. This suggests that the whole temperature distribution changes and that not only the mean shifts towards higher temperatures (Solomon et al. 2007; Franzke 2015).

Quantile regression is also performed on the 45 other cities in Germany, France and Spain (see Tab. 2). A Modified Mann-Kendall trend test reveals statistically significant temperature increases for 46 of the 48 cities in TX and for 44 for TN in all selected percentiles. Trends are not significant in the 50th percentile in Oviedo and Seville for TX and in the 50th percentile in Kiel, Hamburg, Bremen and Córdoba for TN. This shows that for all cities heat stress has already significantly increased over the last few decades. The p-values and Sen's slopes from the Modified Mann-Kendall trend test are summarised for all cities in Tabs. 1-6 in the *Supplementary Material*.

Contrary to E-OBS, trends in the historical RCM simulations are either close to the limit of the significance level of 5% or insignificant. Among the capitals, RCMs provides high confidence in the quantile trends for all used percentiles of TX and TN only in Madrid. TX and TN data are therefore bias-corrected, which improves the results from the models (shown for projections in 2006-2050 in Fig. 4) when compared to E-OBS. Risk is evaluated for all cities through absolute increases of TX and TN in different percentiles. These results suggest that the heat stress risk has significantly increased over the last few decades for all considered cities.

b. Projections of TX and TN in RCMs using RCP2.6 and RCP8.5

Maximum and minimum temperatures are bias-corrected for all 48 locations to generate reliable projections of RCP2.6 and RCP8.5. Increases in the maximum temperature

DRAFT

are found at all locations, for example, in Saarbrücken, Bordeaux and Zaragoza, as displayed in Fig. 4. As for Saarbrücken, the maximum temperature is projected to increase by approximately $3°C$ by 2050 under RACMO RCP8.5 (Fig. 4a). Meanwhile, in Bordeaux, the maximum temperature increases by $3.7°C$ under RCP8.5 using CCLM (Fig. 4b). TX increases even more in Zaragoza: about $4.1°C$ by 2050 under CCLM RCP8.5 (Fig. 4c). Increases in the minimum temperature are also found at all locations, e.g. in Stuttgart, Montpellier and Seville (Fig. 5). As for Stuttgart, the temperature of the city is projected to increase by approximately $2.6°C$ until 2050 under RACMO RCP8.5 (Fig. 5a). Meanwhile, in Montpellier, the minimum temperature increases by $4.4°C$ under RACMO RCP8.5 (Fig. 5b). TN increases also in Seville: about $3.7°C$ by 2050 under REMO2009 RCP8.5 (Fig. 5c). All bias-corrected model temperatures show significant increases in temperature for the considered cities, which implies also increased heat stress risk.

c. Historical evaluation of the wet-bulb temperature

As the CCLM model does not provide relative humidity, we focus on the RACMO, REMO2009 and REMO2015 models in the following. We find that for hindcast simulations of TW based on TN does not lead to critical TW values and, thus, do not pose a direct health risk. However, TW values based on TX do lead to critical wet-bulb temperatures. RCMs show the highest health risks for Mainz and Stuttgart; Bordeaux and Montpellier; Valencia and Toledo of at least 7 days of TW in the 1950-2005 period

DRAFT

as shown in Fig. 6. Hence, bias-corrected RCMs reveal a significant increase of the wet-bulb temperature over the last few decades.

d. Wet-bulb temperature in the RCP2.6 and RCP8.5 scenarios

In order to better quantify heat stress risk we define *critical days* as days for which TW exceeds $26°C$. This value is derived from the relationship between temperature and relative humidity, sometimes also referred to as the Heat Index (e.g. Sherwood and Huber 2010; Wehner et al. 2017; DTN 2017; Raymond et al. 2020).

At about $26°C$, fatigue syndromes are likely to appear under long-time exposure to heat or during physical activity. With increasing air temperatures, even low relative humidity values can result in a dangerously high wet-bulb temperature. For example, for $36°C$ and about 30% of relative humidity, the likelihood to suffer a heat stroke or to be affected by heat exhaustion is 10% higher than for a temperature of $26°C$ and 30% of relative humidity (DTN 2017).

All considered cities experienced increasing numbers of critical days over the period 1950-2005 (Fig. 6). The largest increases can be seen in Spain, followed by France while German cities experienced the smallest increases overall. While there is RCM to RCM variation, the overall ranking of the cities is relatively robust between the RCMs with Valencia, Bordeaux and Stuttgart experiencing the largest increases. On the other hand the cities of Kiel, Nice and Santander saw the smallest increases in the number of critical days (Fig. 6).

DRAFT

We show the corresponding time series of critical days for Saarbrücken, Bordeaux and Zaragoza in Fig. 7. RCMs suggest an increasing number of critical days until 2050 for RCP8.5 when compared to RCP2.6. Critical days are found at all locations by 2050 in RACMO. REMO2009 shows only small insignificant differences between the RCP2.6 and RCP8.5 projections for 3 out of 12 cities in France and for 9 out of 18 cities in Spain. The wet-bulb temperature TW computed from the daily minimum temperature TN does not reach values which would pose a risk to human health for both RCP2.6 and RCP8.5 scenarios. This is because TN increases rather slowly. This suggests, that while the number of critical days is increasing in all considered cities, there is still uncertainty in the precise risk increase, since the different RCMs produce different increasing trends.

TW values above the human tolerance limit of $35°C$ are crossed in all bias-corrected RCMs and in both RCP2.6 and RCP8.5 projections for Berlin and Paris. In Madrid, overall TW values are slightly lower, but still cross a level of $32°C$ in the RCP8.5 projections but not in RCP2.6. A TW temperature above $32°C$ also leads to severe heat stress and can be lethal. This shows that most physical activity becomes unsafe under the RCP8.5 emission scenario.

The distributions of the wet-bulb temperature TW are significantly changing when comparing the periods 2009-2019 with 2040-2050 (Fig. 1 in *Supplementary Material*). The number of very high TW days is increasing in the future projections in all RCM projections. By 2050 both scenarios project maximum daily wet-bulb temperatures for German cities of about $37°C$ averaged over all cities in both RACMO and REMO2009 with a maximum of $43°C$ in Nuremberg. The 95th percentile increases from about $27°C$

DRAFT

in the period 2009-2019 to about 30°C in the period 2040-2050. For French cities, the maximum daily wet-bulb temperature reaches about 36°C in the RACMO projections and 38°C in REMO2009 averaged over all cities. The maximum is reached in Toulouse with 43°C. Again, by 2050 there is not much difference between the RCP2.6 and RCP8.5 projections. The 95th percentile increases from about 27°C in the period 2009-2019 to 31°C in the period 2040-2050. For Spanish cities, again REMO2009 projects somewhat higher average wet-bulb temperatures of about 39°C than RACMO with about 37°C. The highest projected wet-bulb temperatures are in Bilbao of about 45°C. Regarding the change in the 95th percentile averaged over all cities we see an increase from 29°C to 32°C in the latter period. These maximum wet-bulb temperatures suggest that the heat mortality risk is increasing and reaches dangerous levels in both scenarios by 2050.

e. Heat mortality projections

We compute heat mortality projections, by deriving them from daily TX observations and excess deaths during the summer season in Germany, France and Spain in 1950-2018 with total excess deaths and normalized deaths shown in Fig. 8. Excess mortality describes the total number of additional deaths under extreme conditions, for example, during long-lasting heat waves. We define here excess mortality as the number of deaths which are above the regression line. This avoids having to define a fixed time scale (e.g. Huynen et al. 2001; Dushoff et al. 2006) over which to define excess deaths and also takes account of long term changes in the total number of deaths. Overall, excess mortality rates are highest in Germany, followed by France and Spain, where rates are

DRAFT

the lowest (Fig. 8a). Normalized deaths show large variability over Spain, but a few characteristic peaks over Germany and France when heat mortality risk was high (Fig. 8b). It appears that the number of years in which there have been more heat deaths has increased significantly over Spain since the 1990s (Fig. 8b).

In Berlin, the RCP scenarios show small insignificant differences between RCP2.6 and RCP8.5. However, there is a tendency visible that in the French and Spanish capital cities the heat death risk increases by at least 50% in the RCP8.5 scenario compared to the RCP2.6 scenario. For RCP8.5, heat deaths increase by 0.06 deaths/100.000 inhabitants in Paris and by 0.35 deaths/100.000 inhabitants in Madrid, while they increase by just about half that rate for RCP2.6 with 0.03 deaths/100.000 inhabitants in Paris and 0.14 deaths/100.000 inhabitants in Madrid. These findings are consistent with previous studies that find that heat mortality is higher in the Mediterranean than in Northern and Central European countries (D'Ippoliti et al. 2010; Smid et al. 2019).

Almost all cities will experience increases of heat deaths in RCP8.5 compared to RCP2.6 as shown in Fig. 9 and Tab. 3. In Germany (Fig. 9a), a few hot spots seem to emerge in the Frankfurt/Main–Mainz area, and generally, more in southern than in northern Germany. In France, the largest increase in heat deaths per 100.000 inhabitants is concentrated on Paris, Lille and Nice (Fig. 9b). Heat deaths are increasing over Spain (Fig. 9c) especially in the Southern cities of Murcia and Málaga, as well as in Central Spain (Madrid, Toledo) and also partly in the North, in Santander. In summary, all cities are expected to see an increase in heat mortality by 2050 in both scenarios.

DRAFT

4. Conclusions

In this study, we carried out a trend analysis on the projected heat stress and mortality risk in major European cities. Our systematic health risk assessment was based on future regional climate projections for the RCP2.6 and RCP8.5 scenarios. Our three major aims were (i) the evaluation of daily maximum (TX) and daily minimum (TN) temperatures to investigate trends in specific quantiles observed in 1950-2018, (ii) the analysis of an empirically modeled wet-bulb temperature (TW) (Stull 2011) in observations and future projections and (iii) combining temperature and mortality observations to investigate how projections of heat deaths will impact human health until 2050.

From the results of the trend analysis it emerges that E-OBS shows robust increasing trends for summer daily maximum and minimum temperatures. This indicates that historical and present-day trends can spatially be detected by a standardized grid-box approach. RCMs, on the contrary, show only significant trends in all percentiles of TX and TN for Madrid among the capital cities. For most cities, RCM data appear to be stationary, and are rarely consistent with observations. Consequently, the raw RCM data were bias-corrected. This calls for improvements in RCMs to better capture the observed temperature trends for TX and TN.

Significant trends of bias-corrected TX and TN were detected at almost all locations and throughout 1950-2050. Unsurprisingly, TX and TN are estimated to increase more under RCP8.5 than under RCP2.6 during the period 2020-2050. From the modified Mann-Kendall trend test it emerges that low p-values are achieved particularly in observations and in bias-corrected data, which denotes statistically significant increasing

DRAFT

trends for the studied cities that are consistent with various IPCC reports (Smith et al. 2014; Masson-Delmotte et al. 2018).

In this study, TX and TN were used as heat mortality risk parameters instead of the mean temperature. RCMs show an increasing number of critical days until 2050 for RCP8.5 when compared to RCP2.6. Critical days are days for which TW exceeds $26°C$. These findings match a study by Coffel et al. (2017). The number of critical days are found to increase at all locations by 2050 in RACMO. REMO2009 shows only small insignificant differences between the RCP2.6 and RCP8.5 projections for 3 out of 12 cities in France and for 9 out of 18 cities in Spain. This shows the intrinsic uncertainty of RCM projections.

Projections of TW values, computed from the daily maximum temperatures TX, cross the values of $32°C$ and $35°C$ regularly by 2050 in both RCP2.6 and 8.5 scenarios. This is the case for all RCM simulations, making this a robust result. RCMs also share the result that heat stress is projected to increase especially over France, reaching new TW records beyond $35°C$ by 2050. The wet-bulb temperature TW computed from the daily minimum temperature TN, which characterizes night time conditions, does not reach values which would pose a risk to human health for both RCP2.6 and RCP8.5 scenarios. These results illustrate the importance of the wet-bulb temperature since any physical activity would become unsafe above $35°C$. This raises the prospect that by 2050 there will be regular periods when most outdoor physical activities become dangerous and have to be stopped.

DRAFT

Additionally, heat death risk was computed performing linear regression on TX and mortality data, dependent on the country, to dissolve regional differences in heat deaths. Heat mortality increases by up to 0.9%/decade in Germany, 1.7%/decade in France and 7.9%/decade in Spain under RCP8.5. On average, we find that the heat death increase under RCP8.5 is twice the rate as under RCP2.6 in all three countries. Ultimately, the number of heat deaths is expected to increase significantly in RCP8.5 for cities in Central and Southern Germany, Spain and at a few selected hot spots in France. A trend of higher heat mortality was observed over more regional cities. Yet, the capital cities are likely larger heat islands than regional cities because they are larger, have more residents and a higher population density, but there may be fewer deaths. It is likely that capital cities have much greater medical and public facilities than regional cities and are, thus, more likely to mitigate climate risk to a larger extent. The findings are consistent with previous studies (e.g. Gasparrini et al. 2017; Orlov et al. 2019; Watts et al. 2018, 2019; Wolf and McGregor 2013; Yin et al. 2019). The projected changes in regional mortality variation could also be attributable to trends of individual regional conditions, which might be of a socio-economic nature. The projected differences in regional mortality in France indicate similar causes to those in Germany.

Generally, heat-related mortality seems to be higher in Southern German regions than in Northern German regions. The results appear to be sensible compared to the individual increase in the maximum temperatures. In Germany, certain hot spots seem to emerge along the Rhine and Main rivers (e.g. Düsseldorf, Frankfurt/Main and Mainz). Heat-related mortality is also higher in Middle Franconia (e.g. Nuremberg)

DRAFT

than in the Thuringian Basin (e.g. Erfurt). Eastern Germany (e.g. Potsdam, Dresden) is characterised by lower mortality; which might be due to the cities being smaller and their lower population density. As for France, the most noticeable regions regarding higher heat-related mortality are the South (e.g. Nice) and equally, the North (e.g. Lille). This two-parted trend is also visible over Spain. In Spain, mortality is severely increasing in all regions but the focus is set on Andalusia (e.g. Málaga, Seville and Córdoba) and Northern regions. We assume that the reasons for the enhanced mortality are diverse; a mix of socio-economic factors along with an increase in seasonal temperatures.

A potential weakness of our study is the reliance of our heat mortality indicator on a linear regression approach of total mortality against temperature. Unfortunately, heat deaths (WHO code X30) are reported for just the most recent years; for example X30, the exposure to excessive natural heat, is available from 2015, and T67, the effects of heat and light (including heat edema), from 2019. This is too short for a reliable analysis. However, a hindcast test of our regression model validated against reported heat wave deaths, X30, showed reasonably good skill, suggesting that our simple regression approach captures the relationship between wet-bulb temperature and heat deaths. Some of the fluctuations may be a direct result from the regression between monthly deaths and mean TX, for example, internal variability in the data. In the case of Germany, there was a data gap prior to 1990. Despite these fluctuations, the individual regressions provide statistically significant slopes in all three countries, whose long-term behavior is well captured by the model. The constant population may not be too realistic but it can serve as a base line. Therefore, it is possible to approximate heat deaths in cities from this

DRAFT

point of view. We cannot rule out that under the aspect of population change, it could lead to very different results such as an increase in heat mortality due to, for example, a significantly older population in 20 years. As populations fluctuate to some extent, the age distribution of the individual populations may also shift. Hence, the constant population should be treated with caution. In order to better gauge the health impacts of anthropogenic global warming better mortality data is urgently needed, especially longer time series.

As extreme heat also leads to economic losses due to reductions in labor activity and agricultural yield (Orlov et al. 2019; Houser et al. 2015; Carleton and Hsiang 2016; Franzke 2017), future studies are necessary to quantify this effect in the context of a potential increase in heat mortality.

The mean differences in heat mortality increases between RCP2.6 and RCP8.5 over Western Europe show that mitigation efforts have a positive effect in reducing the number of future heat deaths in European cities. This should also be considered in estimations of the social cost of carbon (Nordhaus 2017; Ricke et al. 2018; Pindyck 2019). This would, of course, require the monetization of deaths. However, the social cost of carbon would then be more representative of the true cost of anthropogenic global warming.

Acknowledgments. We thank the three anonymous reviewers and the editor for their helpful comments which helped to improve this manuscript. This study was supported by the Federal Ministry of Education and Research (BMBF) project ClimXtreme and the German Research Foundation (DFG) through the collaborative research center TRR181

DRAFT

– project number 274762653. This work was also supported by the Institute for Basic Science (IBS), Republic of Korea, under IBS-R0278-D1.

Data availability statement. All used data are freely available and the data sources are provided in the text.

References

G. B. Anderson and M. L. Bell. Heat Waves in the United States: Mortality Risk during Heat Waves and Effect Modification by Heat Wave Characteristics in 43 U.S. Communities. *Environ. Health Perspect.*, 119(2):210-218, 2011. doi: 10.1289/ehp.1002313. URL https://www.ncbi.nlm.nih.gov/pmc/articles/PMC3040608/.

D. O. Åström, B. Forsberg, and J. Rocklöv. Heat wave impact on morbidity and mortality in the elderly population: A review of recent studies. *Maturitas*, 69(2011):99-105, 2011.

J.-F. Bastin, E. Clark, T. Elliott, S. Hart, J. van den Hoogen, I. Hordijk, H. Ma, S. Majumder, G. Manoli, J. Maschler, L. Mo, D. Routh, K. Yu, C. M. Zohner, and T. W. Crowther. Understanding climate change from a global analysis of city analogues. *PLoS ONE*, 7(2019):e0217592, 2019.

Bündnis Entwicklung Hilft. *WorldRiskIndex* - The WorldRiskReport, weltrisikobericht.de. https://www.weltrisikobericht.de/english-2/, 2019. 02.03.2020.

DRAFT

T. A. Carleton and S. M. Hsiang. Social and economic impacts of climate. *Science*, 353 (6304):aad9837, 2016.

T. A. Carleton, A. Jina, M. T. Delgado, M. Greenstone, T. Houser, S. M. Hsiang, A. Hultgren, R. E. Kopp, K. E. McCusker, I. B. Nath, et al. Valuing the global mortality consequences of climate change accounting for adaptation costs and benefits. Technical report, National Bureau of Economic Research, 2020.

Centre for Research on the Epidemiology of Disasters (CRED). *The International Disaster Database* - Centre for Research on the Epidemiology of Disasters (CRED), emdat.be. https://www.emdat.be/emdat_db/, 2019. 02.03.2020.

S. Chatterjee and A. S. Hadi. Regression Analysis by Example. *New York: Wiley*, 1(2000):21-50, 2000.

Climate Service Center Germany (GERICS). *Bundesländer-Check, Climate Signal Maps - Regional and Global, Rain Map* - maps and visualizations, products, climate-service-center.de. https://www.climate-service-center.de/products_and_publications/maps_visualisation/index.php.en, 2019. 02.03.2020.

E. D. Coffel, R. M. Horton, and A. de Sherbinin. Temperature and humidity based projections of a rapid rise in global heat stress exposure during the 21st century. *Environ. Res. Lett.*, 13(1):aaa00e, 2017.

S. Coles. An Introduction to Statistical Modeling of Extreme Values. *Springer-Verlag London*, 1(2001):219, 2001.

DRAFT

Copernicus Climate Change Service (C3S). *E-OBS data files 1950-01-01 - 2018-12-31* - data access. `http://c3surf.knmi.nl/dataaccess/access\_eobs.php\#datafiles`, 2019. 02.03.2020.

R. C. Cornes, G. van der Schrier, E. J. M. van den Besselaar, and P. D. Jones. An ensemble version of the E-OBS temperature and precipitation data sets. *J. Geophys. Res.*, 123(17):9391–9409, 2018.

R. E. Davis, G. R. McGregor, and K. B. Enfield. Humidity: A review and primer on atmospheric moisture and human health. *Environ. Res.*, 144(1):106–116, 2016.

M. Dell, B. F. Jones, and B. A. Olken. What Do We Learn from the Weather? The New Climate–Economy Literature. *J. Econ. Lit.*, 52(3):740-798, 2014.

N. Ding, H. L. Berry, and C. M. Bennett. The Importance of Humidity in the Relationship between Heat and Population Mental Health: Evidence from Australia. *PLoS ONE*, 11(10):1–15, 2016.

D. D'Ippoliti, P. Michelozzi, C. Marino, F. de'Donato, B. Menne, K. Katsouyanni, U. Kirchmayer, A. Analitis, M. Medina-Ramón, A. Paldy, R. Atkinson, S. Kovats, L. Bisanti, A. Schneider, A. Lefranc, C. Iñiguez, and C. A. Perucci. The impact of heat waves on mortality in 9 European cities: results from the EuroHEAT project. *Environ. Health*, 9(37):1–9, 2010.

R. V. Donner, R. Ehrcke, S. M. Barbosa, J. Wagner, J. F. Donges, and J. Kurths. Spatial patterns of linear and nonparametric long-term trends in Baltic sea-level variability. *Nonlinear Proc. Geophys.*, 19(1):95–111, 2012.

DRAFT

DTN. Forget Heat Index. Wet Bulb Globe Temperature Is Where It's At. https://www.dtn.com/forget-heat-index-wet-bulb-globe-temperature-is-where-its-at/, 2017. 13.08.2020.

J. Dushoff, J. B. Plotkin, C. Viboud, D. J. D. Earn, and L. Simonsen. Mortality due to influenza in the United States—an annualized regression approach using multiple-cause mortality data. *Amer. J. Epidem.*, 163(2):181–187, 2006.

Ecologistas en Acción. *The Effects of Climate Change on the Risk of Floods in Spain* - ecologistasenaccion.org. https://www.ecologistasenaccion.org/IMG/pdf/informe-inundaciones_cc-ingles.pdf, 2019. 02.03.2020.

EURO-CORDEX initiative. *CORDEX data files 1950-01-01 - 2050-12-31* - data access. https://esg-dn1.nsc.liu.se/search/cordex/, 2019. 02.03.2020.

S. Fatichi, S. M. Barbosa, E. Caporali, and M. E. Silva. Deterministic versus stochastic trends: Detection and challenges. *J. Geophys. Res.*, 114(D18), 2009.

M. C. Fitzpatrick and R. R. Dunn. Contemporary climatic analogs for 540 North American urban areas in the late 21st century. *Nature Comm.*, (2019):10-614, 2019.

C. L. E. Franzke and H. Torello i Sentelles. Risk of extreme high fatalities due to weather and climate hazards and its connection to large-scale climate variability. *Clim. Change*, 162, 507-525, 2020.

DRAFT

C. L. E. Franzke, S. Barbosa, R. Blender, H.-B. Fredriksen, T. Laepple, F. Lambert, T. Nilsen, K. Rypdal, M. Rypdal, M. G. Scotto, S. Vannitsem, N. W. Watkins, L. Yang, and N. Yuan. The structure of climate variability across scales. *Rev. Geophys.*, page e2019RG000657, 2020.

C. L. E. Franzke. Nonlinear trends, long-range dependence, and climate noise properties of surface temperature. *J. Climate*, 25(12):4172–4183, 2012.

C. L. E. Franzke. Local trend disparities of European minimum and maximum temperature extremes. *Geophys. Res. Lett.*, 42(15):6479-6484, 2015.

C. L. E. Franzke. Impacts of a Changing Climate on Economic Damages and Insurance. *Econ. Disas. Clim. Change*, 1(2017):95-110, 2017.

M. Gao and C. L. E. Franzke. Quantile Regression-Based Spatiotemporal Analysis of Extreme Temperature Change in China. *J. Climate*, 30(2017):9897-9914, 2017.

Gasparrini, A., Guo, Y., Hashizume, M., Kinney, P. L., Petkova, E. P., Lavigne, E., Zanobetti, A., Schwartz, J. D., Tobias, A., Leone, M., Tong, S., Honda, Y., Kim, H., and Armstrong, B. G. (2015). Temporal Variation in Heat-Mortality Associations: A Multicountry Study. *Environ. Health Perspect.*, 123(11):1200–1207, 2015. doi: doi.org/10.1289/ehp.1409070. URL `https://pubmed.ncbi.nlm.nih.gov/25933359/`.

A. Gasparrini, Y. Guo, F. Sera, A. M. Vicedo-Cabrera, V. Huber, S. Tong, M. de Sousa Zanotti Stagliorio Coelho, P. Hilario, N. Saldiva, E. Lavigne, P. Matus Correa, N. Valdes Ortega, H. Kan, S. Osorio, J. Kyselý, A. Urban, J. J. K. Jaakkola, N. R. I. Ryti,

DRAFT

M. Pascal, P. G. Goodman, A. Zeka, P. Michelozzi, M. Scortichini, M. Hashizume, Y. Honda, M. Hurtado-Diaz, J. Cesar Cruz, X. Seposo, H. Kim, A. Tobias, C. Iñiguez, B. Forsberg, D. O. Åström, M. S. Ragettli, Y. Leon Guo, C.-F. Wu, A. Zanobetti, J. Schwartz, M. L. Bell, T. N. Dang, D. D. Van, C. Heaviside, S. Vardoulakis, S. Hajat, A. Haines, and B. Armstrong. Projections of temperature-related excess mortality under climate change scenarios. *The Lancet*, 1(9):360-367, 2017.

M. B. Gavrilov, S. B. Marković, N. Janc, M. Nikolić, A. Valjarević, B. Komac, M. Zorn, M. Punišić, and N. Bačević. Assessing average annual air temperature trends using the Mann-Kendall test in Kosovo. *Acta Geographica Slovenica*, 58(1):7-25, 2018.

GermanWatch. *Climate Change Performance Index* - indices, publications, germanwatch.org. `https://www.germanwatch.org/en/CCPI`, 2019a. 02.03.2020.

GermanWatch. *Global Climate Risk Index* - indices, publications, germanwatch.org. `https://www.germanwatch.org/en/cri`, 2019b. 02.03.2020.

GoogleMaps. Map data ©2019 Google. `https://www.google.com/maps`, 2019. 02.03.2020.

K. H. Hamed and A. R. Rao. A modified Mann-Kendall trend test for autocorrelated data. *J. Hydrology*, 204(1998):182-196, 1998.

O. Haug, T. L. Thorarinsdottir, S. H. Sørbye, and C. L. E. Franzke. Spatial trend analysis of gridded temperature data at varying spatial scales. *Adv. Stat. Clim., Meteorol. Ocea.*, 6(1):1–12, 2020.

DRAFT

Havenith, G. Temperature regulation, heat balance and climatic stress. *Extreme Weather Events and Public Health Responses*, Springer, 69-80, 2005

E. Hawkins, T. M. Osborne, C. K. Ho, and A. J. Challinor. Calibration and bias correction of climate projections for crop modelling: An idealised case study over Europe. *Agr. and For. Meteo.*, 170(3):19–31, 2013.

T. Houser, S. M. Hsiang, R. Kopp, and K. Larsen. *Economic Risks of Climate Change: An American Prospectus*. Columbia University Press, 2015.

M.-M. Huynen, P. Martens, D. Schram, M. P. Weijenberg, and A. E. Kunst. The impact of heat waves and cold spells on mortality rates in the Dutch population. *Environ. Health Pers.*, 109(5):463–470, 2001.

A. Ishigami, S. Hajat, R. Sari Kovats, L. Bisanti, M. Rognoni, A. Russo, and A. Paldy. An ecological time-series study of heat-related mortality in three European cities. *Environ. Health*, 7(5), 2008. doi: 10.1186/1476-069X-7-5. URL `https://ehjournal.biomedcentral.com/articles/10.1186/1476-069X-7-5`.

E.-S. Im, J. S. Pal, and E. A. B. Eltahir. Deadly heat waves projected in the densely populated agricultural regions of South Asia. *Sci. Adv.*, 3(8), 2017. doi: 10.1126/sciadv.1603322. URL `http://advances.sciencemag.org/content/3/8/e1603322`.

Institut National de la Statistique et des Études Économiques, Paris, France. *La Rubrique Statistiques* - statistiques, insee.fr. `https://www.insee.fr/fr/accueil`, 2019. 02.03.2020.

DRAFT

Instituto Nacional de Estadística, España. *Estadísticas A-Z* - inebase, ine.es. http://www.ine.es/, 2019. 02.03.2020.

Jendritzky, G., Menz, G., Schirmer, H. and Schmidt-Kessen, W. Methodik zur Räumlichen Bewertung der Thermischen Komponente im Bioklima des Menschen *Beiträge der Akademie für Raumforschung und Landesplanung: Hannover, Germany*, Bd. 114, 1990

E. Kalnay and M. Cai. Impact of urbanization and land-use change on climate. *Nature*, 423(6939):528–531, 2003.

S. Kang and E. A. B. Eltahir. North China Plain threatened by deadly heatwaves due to climate change and irrigation. *Nature Comm.*, 9(1):2894, 2018.

Karlsruher Institut für Technologie (KIT). *CEDIM Risk Explorer Germany* - center for disaster management and risk reduction technology (cedim), cedim.kit.edu. http://www.cedim.kit.edu/riskexplorer.php, 2019. 02.03.2020.

M. Kendall. Rank Correlation Methods. *4th ed. London. Charles Griffin*, (4)202, 1975.

V. Kendrovski, M. Baccini, G. Sanchez Martinez, T. Wolf, E. Paunovic, and B. Menne. Quantifying Projected Heat Mortality Impacts under 21st-Century Warming Conditions for Selected European Countries. *Int. J. Environ. Res. Public Health*, 14(7), 2017. doi: 10.3390/ijerph14070729. URL https://www.mdpi.com/1660-4601/14/7/729.

DRAFT

R. Koenker and K. F. Hallock. Quantile Regression. *J. Econ. Pers.*, 15(4):143-156, 2001.

R. Kopp, J. Buzan, and M. Huber. The Deadly Combination of Heat and Humidity. https://www.nytimes.com/2015/06/07/opinion/sunday/the-deadly-combination-of-heat-and-humidity.html, 2015. 02.03.2020.

J. Luterbacher, D. Dietrich, E. Xoplaki, M. Grosjean, and H. Wanner. European seasonal and annual temperature variability, trends, and extremes since 1500. *Science*, 303 (5663):1499–1503, 2004.

H. Mann. Non-parametric test against trend. *Econometrica*, 13:245-259, 1945.

D. Maraun. Bias Correcting Climate Change Simulations - a Critical Review. *Curr. Clim. Change Rep.*, 2(2016):211-220, 2016.

Matzarakis, A., Muthers, S. and Graw, K.. Thermische Belastung von Bewohnern in Städten bei Hitzewellen am Beispiel von Freiburg (Breisgau) *Bundesgesundheitsblatt - Gesundheitsforschung - Gesundheitsschutz*, 63, 1004–1012, 2020.

V. Masson-Delmotte, P. Zhai, H.-O. Pörtner, D. Roberts, J. Skea, P. Shukla, A. Pirani, W. Moufouma-Okia, C. Péan, R. Pidcock, S. Connors, J. Matthews, Y. Chen, X. Zhou, M. Gomis, E. Lonnoy, T. Maycock, M. Tignor, and T. e. Waterfield. IPCC, 2018: Summary for Policymakers. *Global Warming of* 1.5°*C. An IPCC Special Report on the impacts of global warming of* 1.5°*C above pre-industrial levels and related global greenhouse gas emission pathways, in the context of strengthening the global*

DRAFT

response to the threat of climate change, sustainable development, and efforts to eradicate poverty, pages 3–24, 2018.

S. Merte. Estimating heat wave-related mortality in Europe using singular spectrum analysis. *Clim. Change*, 142(3-4):321-330, 2017.

D. Mitchell, K. Kornhuber, C. Huntingford, and P. Uhe. The day the 2003 European heatwave record was broken. *The Lancet*, 3(7):290-292, 2019.

C. Mora, B. Dousset, I. R. Caldwell, F. E. Powell, C. Geronimo, C. R. Bielecki, C. W. W. Counsell, B. S. Dietrich, E. T. Johnston, L. V. Louis, M. P. Lucas, M. M. McKenzie, A. G. Shea, H. Tseng, T. W. Giambelluca, L. R. Leon, E. Hawkins, and C. Trauernicht. Global risk of deadly heat. *Nature Climate Change*, 7(2017):501-506, 2017.

P. Murage, S. Hajat, and R. S. Kovats. Effect of night-time temperatures on cause and age-specific mortality in London. *Environ. Epidem.*, 1(2):e005, 2017.

My Geo Info. *Map of France*. `http://www.mygeo.info/landkarten\_frankreich.html`, 2019. 02.03.2020.

Natural Earth. Europe blank laea location map. `http://naturalearthdata.com/`, 2010. 02.03.2020.

W. D. Nordhaus. Revisiting the social cost of carbon. *Proc. Nat. Acad. Sci. USA*, 114 (7):1518–1523, 2017.

DRAFT

K. W. Oleson, G. B. Bonan, J. Feddema, and T. Jackson. An examination of urban heat island characteristics in a global climate model. *Int. J. Clim.*, 31(12):1848–1865, 2011.

A. Orlov, J. Sillmann, A. Aaheim, K. Aunan, and K. de Bruin. Economic Losses of Heat-Induced Reductions in Outdoor Worker Productivity: a Case Study of Europe. *Econ. Disas. Clim. Change*, 3(2019):191-211, 2019.

J. S. Pal and E. A. B. Eltahir. Future temperature in southwest Asia projected to exceed a threshold for human adaptability. *Nature Climate Change*, 6(2):197, 2016.

R. S. Pindyck. The social cost of carbon revisited. *J. Env. Econ. Manag.*, 94:140–160, 2019.

M. Poumadère, C. Mays, S. Le Mer, and R. Blong. The 2003 Heat Wave in France: Dangerous Climate Change Here and Now. *Risk Analysis*, 25(6):1483-1494, 2005.

C. Raymond, T. Matthews, and R. M. Horton. The emergence of heat and humidity too severe for human tolerance. *Sci. Adv.*, 6(19):1–8, 2020.

K. Ricke, L. Drouet, K. Caldeira, and M. Tavoni. Country-level social cost of carbon. *Nature Climate Change*, 8(10):895–900, 2018.

J.-M. Robine, S. L. K. Cheung, S. Le Roy, H. Van Oyen, C. Griffiths, J.-P. Michel, and F. R. Herrmann. Death toll exceeded 70,000 in Europe during the summer of 2003. *Comptes Rendus Biologies*, 331(2):171–178, 2008.

DRAFT

S. I. Seneviratne, N. Nicholls, D. Easterling, C. M. Goodess, S. Kanae, J. Kossin, Y. Luo, J. Marengo, K. McInnes, M. Rahimi, M. Reichstein, A. Sorteberg, C. Vera, and X. Zhang. Changes in climate extremes and their impacts on the natural physical environment. In C. B. Field, V. Barros, T. Stocker, D. Qin, D. Dokken, K. Ebi, M. Mastrandrea, K. Mach, G. Plattner, S. Allen, M. Tignor, and P. Midgley, editors, *Managing the risks of extreme events and disasters to advance climate change adaptation. A Special Report of Working Groups I and II of the Intergovernmental Panel on Climate Change (IPCC)*, pages 109–230. Cambridge University Press, Cambridge, 2012.

S. C. Sherwood and M. Huber. An adaptability limit to climate change due to heat stress. *Proc. Nat. Acad. Sci. USA*, 107(21):9552–9555, 2010.

M. Smid, S. Russo, A. C. Costa, C. Granell, and E. Pebesma. Ranking European capitals by exposure to heat waves and cold waves. *Urban Clim.*, 27(3):388–402, 2019.

K. Smith, A. Woodward, D. Campbell-Lendrum, D. Chadee, Y. Honda, Q. Liu, J. Olwoch, B. Revich, and R. Sauerborn. Human health: impacts, adaptation, and co-benefits. *Climate Change 2014: Impacts, Adaptation, and Vulnerability. Part A: Global and Sectoral Aspects. Contribution of Working Group II to the Fifth Assessment Report of the Intergovernmental Panel on Climate Change*, pages 709–754, 2014.

Society of Actuaries. *Actuaries Climate Index*. `http://actuariesclimateindex.org/about/`, 2019. 02.03.2020.

DRAFT

S. Solomon, M. Manning, M. Marquis, D. Qin, et al. *Climate Change 2007-The Physical Science Basis: Working group I Contribution to the Fourth Assessment Report of the IPCC*, volume 4. Cambridge University Press, 2007.

Statistisches Bundesamt Deutschland. *Statistical Offices of the German States* - Statistisches Bundesamt Deutschland, destatis.de. https://www.destatis.de/EN/PressServices/AddressBook/National.html, 2019. 02.03.2020.

D. J. Stensrud. *Parameterization schemes: keys to understanding numerical weather prediction models*. Cambridge University Press, 2009.

R. Stull. Wet-Bulb Temperature from Relative Humidity and Air Temperature. *J. Climate*, 50(2011):2267-2269, 2011.

The CGIAR Research Program on Climate Change, Agriculture and Food Security (CCAFS). Bias-Correction. http://ccafs-climate.org/bias_correction/, 2014. 13.08.2020.

N. Todd and A.-J. Valleron. Space-Time Covariation of Mortality with Temperature: A Systematic Study of Deaths in France, 1968-2009. *Environ. Health Perspect.*, 123(7), 2015. doi: 10.1289/ehp.1307771. URL https://pubmed.ncbi.nlm.nih.gov/25803836/.

Umweltbundesamt. Monitoringbericht 2019 zur Deutschen Anpassungsstrategie an den Klimawandel. https://www.umweltbundesamt.de/publikationen/monitoringbericht-2019, 2019. 02.03.2020.

DRAFT

UNEP/GRID-Geneva. *Global Risk Data Platform*. https://preview.grid.unep.ch/index.php?preview=map\&lang=eng, 2019. 02.03.2020.

Y. Wang, A. Wang, J. Zhai, H. Tao, T. Jiang, B. Su, J. Yang, G. Wang, Q. Liu, C. Gao, Z. W. Kundzewicz, M. Zhan, Z. Feng, and T. Fischer. Ten of thousands additional deaths annually in cities of China between 1.5°C and 2°C warming. *Nature Comm.*, (2019):10-3376, 2019.

N. Watts, M. Amann, N. Arnell, S. Ayeb-Karlsson, K. Belesova, H. Berry, T. Bouley, M. Boykoff, P. Byass, W. Cai, D. Campbell-Lendrum, J. Chambers, M. Daly, N. Dasandi, M. Davies, A. Depoux, P. Dominguez-Salas, P. Drummond, K. L. Ebi, P. Ekins, L. Fernandez Montoya, H. Fischer, L. Georgeson, D. Grace, H. Graham, I. Hamilton, S. Hartinger, J. Hess, I. Kelman, G. Kiesewetter, T. Kjellstrom, D. Kniveton, B. Lemke, L. Liang, M. Lott, R. Lowe, M. Odhiambo Sewe, J. Martinez-Urtaza, M. Maslin, L. McAllister, S. Jankin Mikhaylov, J. Milner, M. Moradi-Lakeh, K. Morrissey, K. Murray, M. Nilsson, T. Neville, T. Oreszczyn, F. Owfi, O. Pearman, D. Pencheon, S. Pye, M. Rabbaniha, E. Robinson, J. Rocklov, O. Saxer, S. Schutte, J. C. Semenza, J. Shumake-Guillemot, R. Steinbach, M. Tabatabaei, J. Tomei, J. Trinanes, N. Wheeler, P. Wilkinson, P. Gong, H. Montgomery, and A. Costello. The 2018 report of the Lancet Countdown on health and climate change: shaping the health of nations for centuries to come. *The Lancet*, 392(10163):2479-2514, 2018.

N. Watts, M. Amann, N. Arnell, S. Ayeb-Karlsson, K. Belesova, M. Boykoff, P. Byass, W. Cai, D. Campbell-Lendrum, S. Capstick, J. Chambers, C. Dalin, M. Daly,

DRAFT

N. Dasandi, M. Davies, P. Drummond, R. Dubrow, K. L. Ebi, M. Eckelman, P. Ekins, L. E. Escobar, L. Fernandez Montoya, L. Georgeson, H. Graham, P. Haggar, I. Hamilton, S. Hartinger, J. Hess, I. Kelman, G. Kiesewetter, T. Kjellstrom, D. Kniveton, B. Lemke, Y. Liu, M. Lott, R. Lowe, M. Odhiambo Sewe, J. Martinez-Urtaza, M. Maslin, L. McAllister, A. McGushin, S. Jankin Mikhaylov, J. Milner, M. Moradi-Lakeh, K. Morrissey, K. Murray, S. Munzert, M. Nilsson, T. Neville, T. Oreszczyn, F. Owfi, O. Pearman, D. Pencheon, D. Phung, S. Pye, R. Quinn, M. Rabbaniha, E. Robinson, J. Rocklöv, J. C. Semenza, J. Sherman, J. Shumake-Guillemot, M. Tabatabaei, J. Taylor, J. Trinanes, P. Wilkinson, A. Costello, P. Gong, and H. Montgomery. The 2019 report of the Lancet Countdown on health and climate change: ensuring that the health of a child born today is not defined by a changing climate. *The Lancet*, 394(10211):1836-1878, 2019.

Watts N, Amann M, Arnell N, Ayeb-Karlsson S, Beagley J, Belesova K, Boykoff M, Byass P, Cai W, Campbell-Lendrum D, Capstick S, Chambers J, Coleman S, Dalin C, Daly M, Dasandi N, Dasgupta S, Davies M, Di Napoli C, Dominguez-Salas P, Drummond P, Dubrow R, Ebi KL, Eckelman M, Ekins P, Escobar LE, Georgeson L, Golder S, Grace D, Graham H, Haggar P, Hamilton I, Hartinger S, Hess J, Hsu SC, Hughes N, Jankin Mikhaylov S, Jimenez MP, Kelman I, Kennard H, Kiesewetter G, Kinney PL, Kjellstrom T, Kniveton D, Lampard P, Lemke B, Liu Y, Liu Z, Lott M, Lowe R, Martinez-Urtaza J, Maslin M, McAllister L, McGushin A, McMichael C, Milner J, Moradi-Lakeh M, Morrissey K, Munzert S, Murray KA, Neville T, Nilsson M, Sewe MO, Oreszczyn T, Otto M, Owfi F, Pearman O, Pencheon D, Quinn R,

DRAFT

Rabbaniha M, Robinson E, Rocklöv J, Romanello M, Semenza JC, Sherman J, Shi L, Springmann M, Tabatabaei M, Taylor J, Triñanes J, Shumake-Guillemot J, Vu B, Wilkinson P, Winning M, Gong P, Montgomery H, Costello A. The 2020 report of The Lancet Countdown on health and climate change: responding to converging crises. *The Lancet*, 397(10269):129-170, 2021. doi: 10.1016/S0140-6736(20)32290-X URL https://pubmed.ncbi.nlm.nih.gov/33278353/.

M. Wehner, F. Castillo, and D. Stone. The impact of moisture and temperature on human health in heat waves, 04 2017. URL https://oxfordre.com/naturalhazardscience/view/10.1093/acrefore/9780199389407.001.0001/acrefore-9780199389407-e-58.

T. Wolf and G. McGregor. The development of a heat wave vulnerability index for London, United Kingdom. *Wea. Clim. Extremes*, 1(2013):59-68, 2013.

World Atlas. *Map of Spain*. https://www.worldatlas.com/countries/spain.html, 2019. 02.03.2020.

World of Maps. *Map of Germany*. https://www.worldofmaps.net/europa/deutschland/generelle-karte-deutschland.htm, 2019. 02.03.2020.

Q. Yin, J. Wang, Z. Ren, J. Li, and Y. Guo. Mapping the increased minimum mortality temperatures in the context of global climate change. *Nature Comm.*, 4640(2019):1-8, 2019.

Y. Zhang, I. Held, and S. Fueglistaler. Projections of tropical heat stress constrained by atmospheric dynamics *Nat. Geosci.*, 14(2021):133-137, 2021.

DRAFT

LIST OF TABLES

Table 1. Summary of RCM data from 1950-2005 and 2006-2050 47

Table 2. List of studied cities in Germany, France and Spain sorted by number on the map (Fig. 1). 48

Table 3. Trend slopes and mean difference in heat mortality for future climate projections [in %/decade] derived from daily TX observations and excess deaths in RCP2.6 and RCP8.5 for cities in Germany, France and Spain for the period 2019-2050. 49

Table 4. Coefficients from the quantile regression of seasonal maximum temperatures in Berlin, Paris and Madrid for different percentiles in 1950-2018. 50

Table 5. Coefficients from the quantile regression of seasonal minimum temperatures in Berlin, Paris and Madrid for different percentiles in 1950-2018. 51

Table 6. Coefficients from the heat mortality regression for Germany, France and Spain from June through August in 1950-2018. 52

DRAFT

929 TABLE 1. Summary of RCM data (1950-2005 and 2006-2050) that is available ('x') for historical

930 evaluation and climate projections, with missing data marked as 'na'.

GCM	RCM	RCM	RCP	TX	TN	RH
1950-2050	1950-2005	2006-2050	2006-2050			
EC-EARTH	CCLM	CCLM	2.6, 8.5	x	x	na
EC-EARTH	RACMO	RACMO	2.6, 8.5	x	x	x
MPI-ESM-LR	REMO2009	REMO2009	2.6, 8.5	x	x	x
NorESM1-M	REMO2015	REMO2015	8.5	x	x	x

DRAFT

TABLE 2. List of studied cities in Germany, France and Spain sorted by number on the map (Fig. 1).

No.	Germany	France	Spain	No.	Germany	France	Spain
1	Kiel	Lille	Santiago de Compostela	**10**	Erfurt	Montpellier	Barcelona
2	Hamburg	Rouen	Oviedo	**11**	Dresden	Marseille	Madrid
3	Schwerin	Paris	Santander	**12**	Frankfurt/Main	Nice	Toledo
4	Bremen	Strasbourg	Bilbao	**13**	Wiesbaden	–	Badajoz
5	Berlin	Nantes	Vitoria-Gasteiz	**14**	Mainz	–	Valencia
6	Potsdam	Dijon	Pamplona	**15**	Saarbrücken	–	Córdoba
7	Hanover	Lyon	Logroño	**16**	Nuremberg	–	Seville
8	Magdeburg	Bordeaux	Valladolid	**17**	Stuttgart	–	Málaga
9	Düsseldorf	Toulouse	Zaragoza	**18**	Munich	–	Murcia

DRAFT

931 TABLE 3. Trend slopes and mean difference in heat mortality for future climate projections [in
932 %/decade] derived from daily TX observations and excess deaths in RCP2.6 and RCP8.5 for cities
933 in Germany, France and Spain for the period 2019-2050.

	RCP 2.6	RCP 8.5	mean diff		RCP 2.6	RCP 8.5	mean diff
Berlin	0.34	0.34	0.00	**Madrid**	4.83	11.43	6.6
Bremen	-0.02	0.08	0.09	**Badajoz**	3.28	5.99	2.7
Dresden	0.3	0.3	0.00	**Barcelona**	5.26	7.35	2.09
Düsseldorf	1.05	1.58	0.53	**Bilbao**	5.66	7.95	2.29
Erfurt	0.9	1.12	0.22	**Córdoba**	1.58	4.81	3.24
FrankfurtM	0.73	2.23	1.49	**Logroño**	4.02	7.87	3.85
Hamburg	0.21	0.52	0.3	**Málaga**	3.4	12.41	9.01
Hanover	0.09	0.68	0.59	**Murcia**	7.89	12.67	4.79
Kiel	-0.12	0.12	0.24	**Oviedo**	-0.55	0.83	1.38
Magdeburg	0.59	1.06	0.48	**Pamplona**	3.05	6.37	3.33
Mainz	0.75	1.95	1.21	**Santander**	8.74	12.59	3.85
Munich	0.67	1.01	0.34	**Santiago de Compostela**	2.48	4	1.52
Nuremberg	0.35	1.4	1.05	**Seville**	1.58	6.28	4.7
Potsdam	0.07	0.11	0.04	**Toledo**	6.81	9.84	3.03
Saarbrücken	0.76	1.28	0.51	**Valencia**	7.12	9.59	2.48
Schwerin	0.14	0.51	0.37	**Valladolid**	5.31	9.02	3.71
Stuttgart	0.66	1.06	0.41	**Vitoria-Gasteiz**	3.22	6.87	3.65
Wiesbaden	0.58	0.93	0.35	**Zaragoza**	5.36	6.94	1.57
total Germany	0.45	0.9	0.46	**total Spain**	4.39	7.93	3.54
Paris	1.21	2.1	0.89				
Bordeaux	0.85	1.49	0.65				
Dijon	0.88	1.79	0.91				
Lille	1.27	1.93	0.66				
Lyon	1	1.7	0.7				
Marseille	1.22	1.65	0.44				
Montpellier	1.36	1.86	0.5				
Nantes	1.02	1.86	0.84				
Nice	0.7	1.91	1.21				
Rouen	0.51	1.22	0.71				
Strasbourg	0.87	1.33	0.46				
Toulouse	0.66	1.43	0.76				
total France	0.96	1.69	0.73				

DRAFT

934 TABLE 4. Coefficients from the quantile regression of seasonal maximum temperatures in Berlin,

935 Paris and Madrid for different percentiles in 1950-2018.

Berlin	Estimate	Std. Error	t value	Pr(>t)	Multiple R-squared	Adjusted R-squared	F-statistic	p-value
Slope (50th percentile)	0.03	0.08	4.18	$8 \cdot 10^{-5}$	0.2	0.19	17.48	$8 \cdot 10^{-5}$
Slope (80th percentile)	0.04	$9 \cdot 10^{-3}$	4.17	$8 \cdot 10^{-5}$	0.2	0.19	17.41	$8 \cdot 10^{-5}$
Slope (90th percentile)	0.04	$9 \cdot 10^{-3}$	4.94	$5 \cdot 10^{-6}$	0.26	0.25	24.47	$5 \cdot 10^{-6}$
Slope (95th percentile)	0.04	$9 \cdot 10^{-3}$	4.45	$3 \cdot 10^{-5}$	0.22	0.21	19.86	$3 \cdot 10^{-5}$
Paris	Estimate	Std. Error	t value	Pr(>t)	Multiple R-squared	Adjusted R-squared	F-statistic	p-value
Slope (50th percentile)	0.04	$8 \cdot 10^{-3}$	5.26	$1 \cdot 10^{-6}$	0.29	0.28	27.7	$1 \cdot 10^{-6}$
Slope (80th percentile)	0.05	$9 \cdot 10^{-3}$	5.36	$1 \cdot 10^{-6}$	0.3	0.28	28.77	$1 \cdot 10^{-6}$
Slope (90th percentile)	0.05	0.01	4.38	$4 \cdot 10^{-5}$	0.22	0.21	19.24	$4 \cdot 10^{-5}$
Slope (95th percentile)	0.05	0.01	4.28	$6 \cdot 10^{-5}$	0.21	0.2	18.35	$6 \cdot 10^{-5}$
Madrid	Estimate	Std. Error	t value	Pr(>t)	Multiple R-squared	Adjusted R-squared	F-statistic	p-value
Slope (50th percentile)	0.04	$7 \cdot 10^{-3}$	6.9	$2 \cdot 10^{-9}$	0.41	0.4	47.71	$2 \cdot 10^{-9}$
Slope (80th percentile)	0.04	$5 \cdot 10^{-3}$	8.11	$1 \cdot 10^{-11}$	0.49	0.48	65.9	$1 \cdot 10^{-11}$
Slope (90th percentile)	0.04	$5 \cdot 10^{-3}$	8.93	$5 \cdot 10^{-13}$	0.54	0.53	79.82	$5 \cdot 10^{-13}$
Slope (95th percentile)	0.04	$5 \cdot 10^{-3}$	8.42	$4 \cdot 10^{-12}$	0.51	0.5	71	$4 \cdot 10^{-12}$

DRAFT

936 TABLE 5. Coefficients from the quantile regression of seasonal minimum temperatures in Berlin,
937 Paris and Madrid for different percentiles in 1950-2018.

Berlin	Estimate	Std. Error	t value	Pr(>t)	Multiple R-squared	Adjusted R-squared	F-statistic	p-value
Slope (50th percentile)	0.02	$4 \cdot 10^{-3}$	4.37	$4 \cdot 10^{-5}$	0.22	0.21	19.09	$4 \cdot 10^{-5}$
Slope (80th percentile)	0.02	$5 \cdot 10^{-3}$	5.01	$4 \cdot 10^{-6}$	0.27	0.26	25.17	$4 \cdot 10^{-6}$
Slope (90th percentile)	0.02	$5 \cdot 10^{-3}$	4.51	$2 \cdot 10^{-5}$	0.23	0.22	20.34	$2 \cdot 10^{-5}$
Slope (95th percentile)	0.02	$6 \cdot 10^{-3}$	4.38	$4 \cdot 10^{-5}$	0.22	0.21	19.23	$4 \cdot 10^{-5}$
Paris	Estimate	Std. Error	t value	Pr(>t)	Multiple R-squared	Adjusted R-squared	F-statistic	p-value
Slope (50th percentile)	0.03	$4 \cdot 10^{-3}$	7.09	$1 \cdot 10^{-9}$	0.42	0.42	50.33	$1 \cdot 10^{-9}$
Slope (80th percentile)	0.03	$5 \cdot 10^{-3}$	7.07	$1 \cdot 10^{-9}$	0.42	0.41	50.07	$1 \cdot 10^{-9}$
Slope (90th percentile)	0.03	$6 \cdot 10^{-3}$	6.27	$2 \cdot 10^{-8}$	0.37	0.36	39.42	$2 \cdot 10^{-8}$
Slope (95th percentile)	0.03	$6 \cdot 10^{-3}$	6.29	$2 \cdot 10^{-8}$	0.37	0.36	39.66	$2 \cdot 10^{-8}$
Madrid	Estimate	Std. Error	t value	Pr(>t)	Multiple R-squared	Adjusted R-squared	F-statistic	p-value
Slope (50th percentile)	0.03	$6 \cdot 10^{-3}$	6.17	$4 \cdot 10^{-8}$	0.36	0.35	38.17	$4 \cdot 10^{-8}$
Slope (80th percentile)	0.03	$5 \cdot 10^{-3}$	7.08	$1 \cdot 10^{-9}$	0.42	0.41	50.15	$1 \cdot 10^{-9}$
Slope (90th percentile)	0.04	$5 \cdot 10^{-3}$	7.81	$5 \cdot 10^{-11}$	0.47	0.46	61.06	$5 \cdot 10^{-11}$
Slope (95th percentile)	0.04	$5 \cdot 10^{-3}$	8.19	$1 \cdot 10^{-11}$	0.5	0.49	67.19	$1 \cdot 10^{-11}$

DRAFT

938 TABLE 6. Coefficients from the heat mortality regression for Germany, France and Spain from
939 June through August in 1950-2018.

Germany	Estimate	Std. Error	t value	Pr(>t)	Multiple R-squared	Adjusted R-squared	F-statistic	p-value
Slope	0.18	0.03	5.17	$2.23 \cdot 10^{-6}$	0.28	0.27	26.81	$2.23 \cdot 10^{-6}$
France	Estimate	Std. Error	t value	Pr(>t)	Multiple R-squared	Adjusted R-squared	F-statistic	p-value
Slope	25.99	5.74	4.52	$2.52 \cdot 10^{-5}$	0.23	0.22	20.49	$2.51 \cdot 10^{-5}$
Spain	Estimate	Std. Error	t value	Pr(>t)	Multiple R-squared	Adjusted R-squared	F-statistic	p-value
Slope	84.45	10.7	7.89	$3.74 \cdot 10^{-11}$	0.48	0.47	62.31	$3.73 \cdot 10^{-11}$

DRAFT

LIST OF FIGURES

Fig. 1. Selected cities in Germany (black numbers), in France (blue) and in Spain (orange). See Tab. 2 for city names (Map sources: Natural Earth (2010); GoogleMaps (2019)). 54

Fig. 2. Linear regression fits (blue line) between deaths and seasonal maximum temperatures TX for a) Germany, b) France and c) Spain from June through August in 1950-2018. 55

Fig. 3. Quantile regression trends for seasonal maximum temperatures TX (left row) and seasonal minimum temperatures TN (right row) for a) Berlin, b) Paris and c) Madrid for different percentiles in 1950-2018. 56

Fig. 4. Quantile regression trends of seasonal maximum temperatures TX for scenarios RCP2.6 and RCP8.5 of a) Saarbrücken RACMO RCP2.6, b) RCP8.5, c) Bordeaux CCLM RCP2.6, d) RCP8.5 and e) Zaragoza CCLM RCP2.6 and f) RCP8.5 for different percentiles in 2006-2050. For the quantile regression bias-corrected RCM temperatures have been used. 57

Fig. 5. Quantile regression trends of seasonal minimum temperatures TN for scenarios RCP2.6 and RCP8.5 of a) Stuttgart RACMO RCP2.6 b) RCP8.5, c) Montpellier RACMO RCP2.6, d) RCP8.5 and e) Seville REMO2009 RCP2.6 and f) RCP8.5 for different percentiles in 2006-2050. For the quantile regressions bias-corrected RCM temperatures have been used. 58

Fig. 6. Increase in the number of critical TW days in a) German, b) French and c) Spanish cities over the period 1950-2005. 59

Fig. 7. Seasonal wet-bulb temperatures TW for scenarios RCP2.6 and RCP8.5 with linear regression trend (red line) of a) Saarbrücken RACMO RCP2.6 b) RCP8.5, c) Bordeaux RACMO RCP2.6, d) RCP8.5 and e) Zaragoza REMO2009 RCP2.6 and f) RCP8.5 for different percentiles in 2006-2050. 60

Fig. 8. Excess heat deaths per 100.000 residents with regression line (left) and normalized (detrended) excess heat heat deaths (right) in Germany, France and Spain in 1950-2018. 61

Fig. 9. Trend slope of heat mortality for future climate projections [in %/decade] derived from daily TX observations and excess deaths in RCP8.5 for cities in a) Germany, b) France and c) Spain in 2019-2050 (Map sources: World of Maps (2019), My Geo Info (2019), World Atlas (2019)). 62

DRAFT

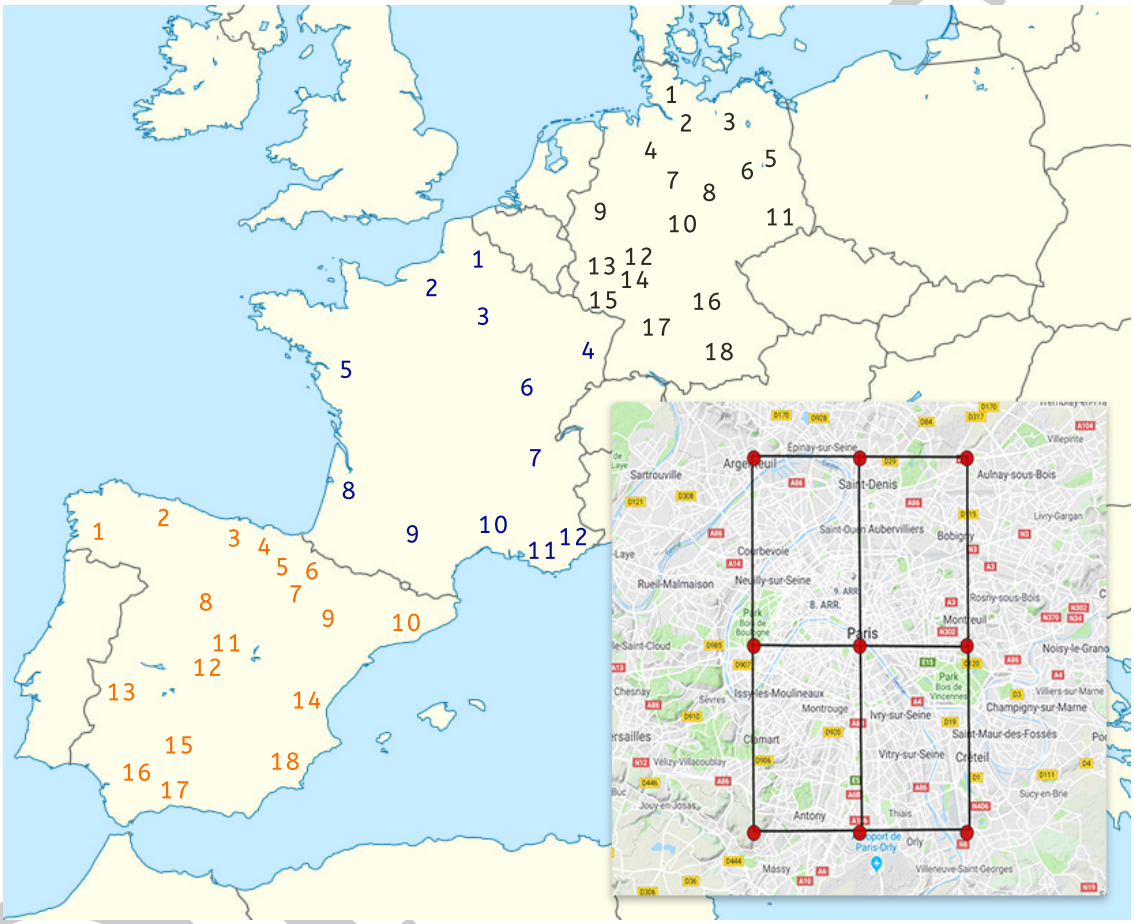

FIG. 1. Selected cities in Germany (black numbers), in France (blue) and in Spain (orange). See Tab. 2 for city names (Map sources: Natural Earth (2010); GoogleMaps (2019)).

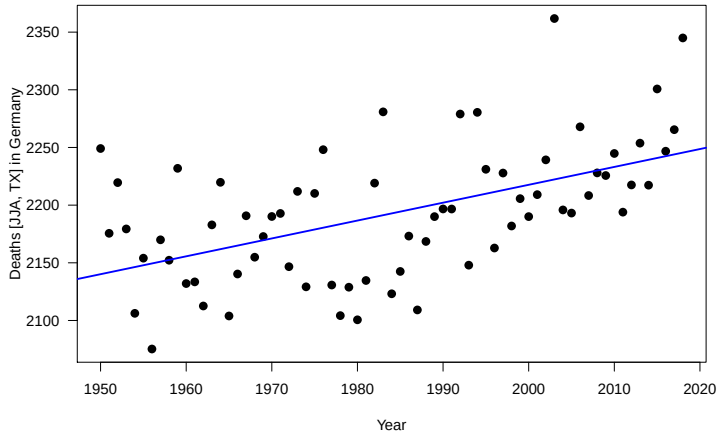

a)

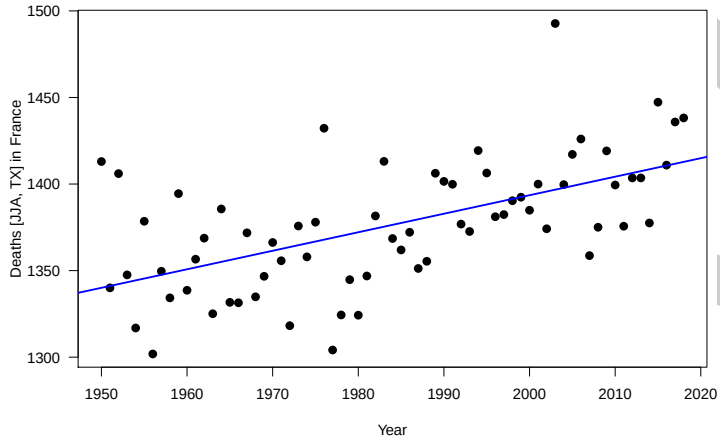

b)

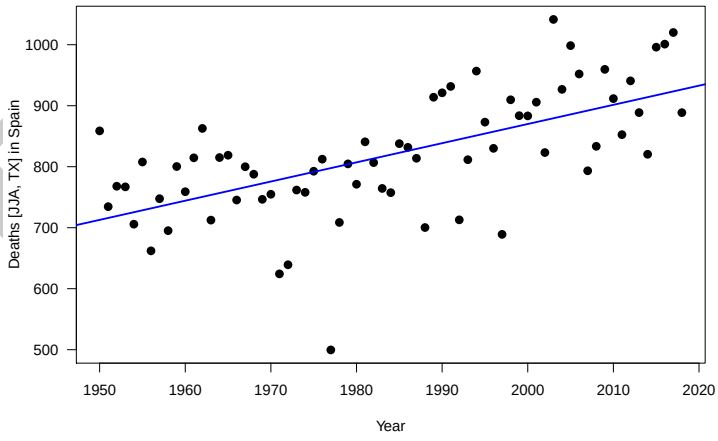

c)

975 FIG. 2. Linear regression fits (blue line) between deaths and seasonal maximum temperatures TX
976 for a) Germany, b) France and c) Spain from June through August in 1950-2018.

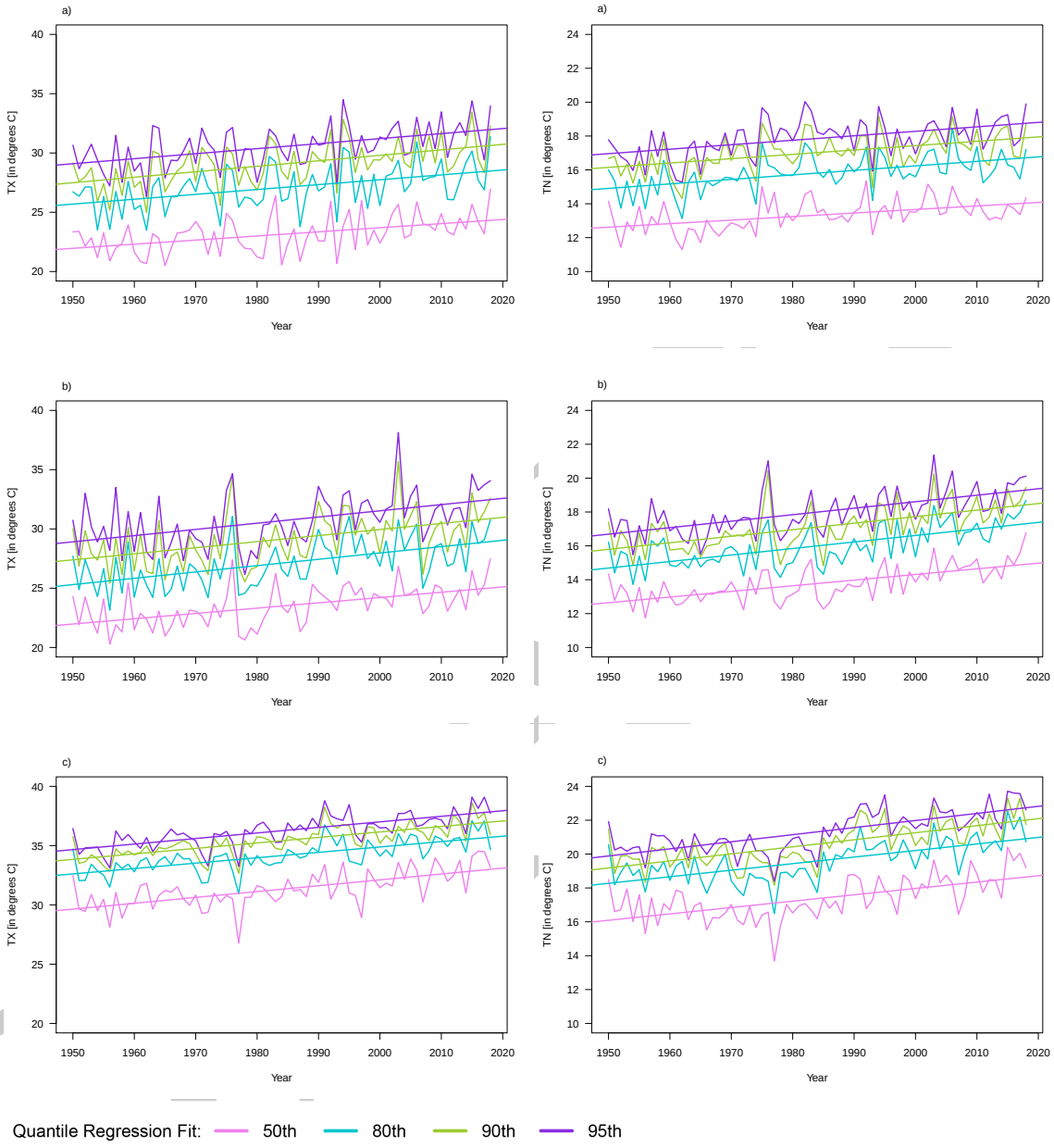

977 FIG. 3. Quantile regression trends for seasonal maximum temperatures TX (left row) and seasonal
978 minimum temperatures TN (right row) for a) Berlin, b) Paris and c) Madrid for different percentiles
979 in 1950-2018.

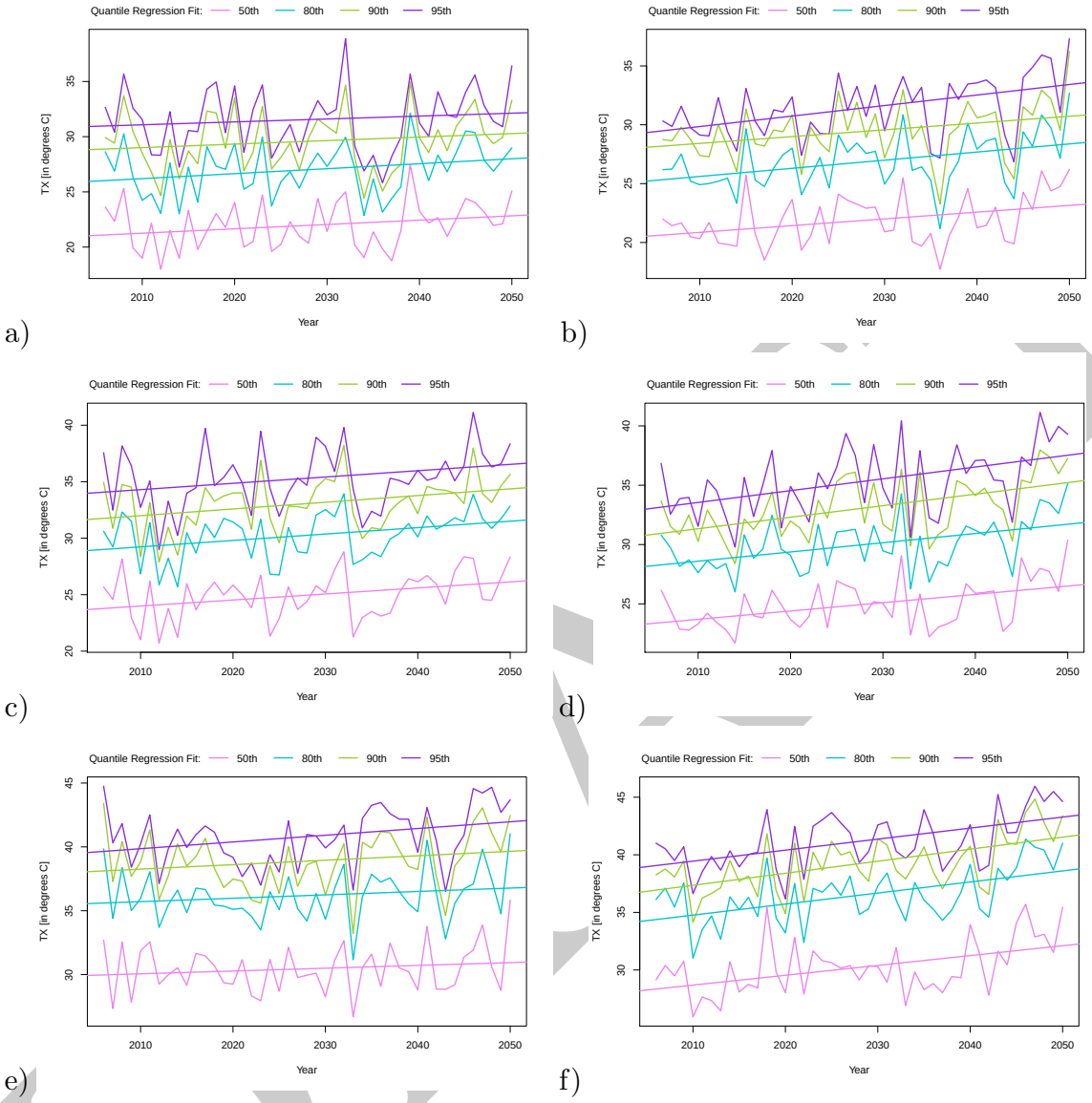

FIG. 4. Quantile regression trends of seasonal maximum temperatures TX for scenarios RCP2.6 and RCP8.5 of a) Saarbrücken RACMO RCP2.6, b) RCP8.5, c) Bordeaux CCLM RCP2.6, d) RCP8.5 and e) Zaragoza CCLM RCP2.6 and f) RCP8.5 for different percentiles in 2006-2050. For the quantile regression bias-corrected RCM temperatures have been used.

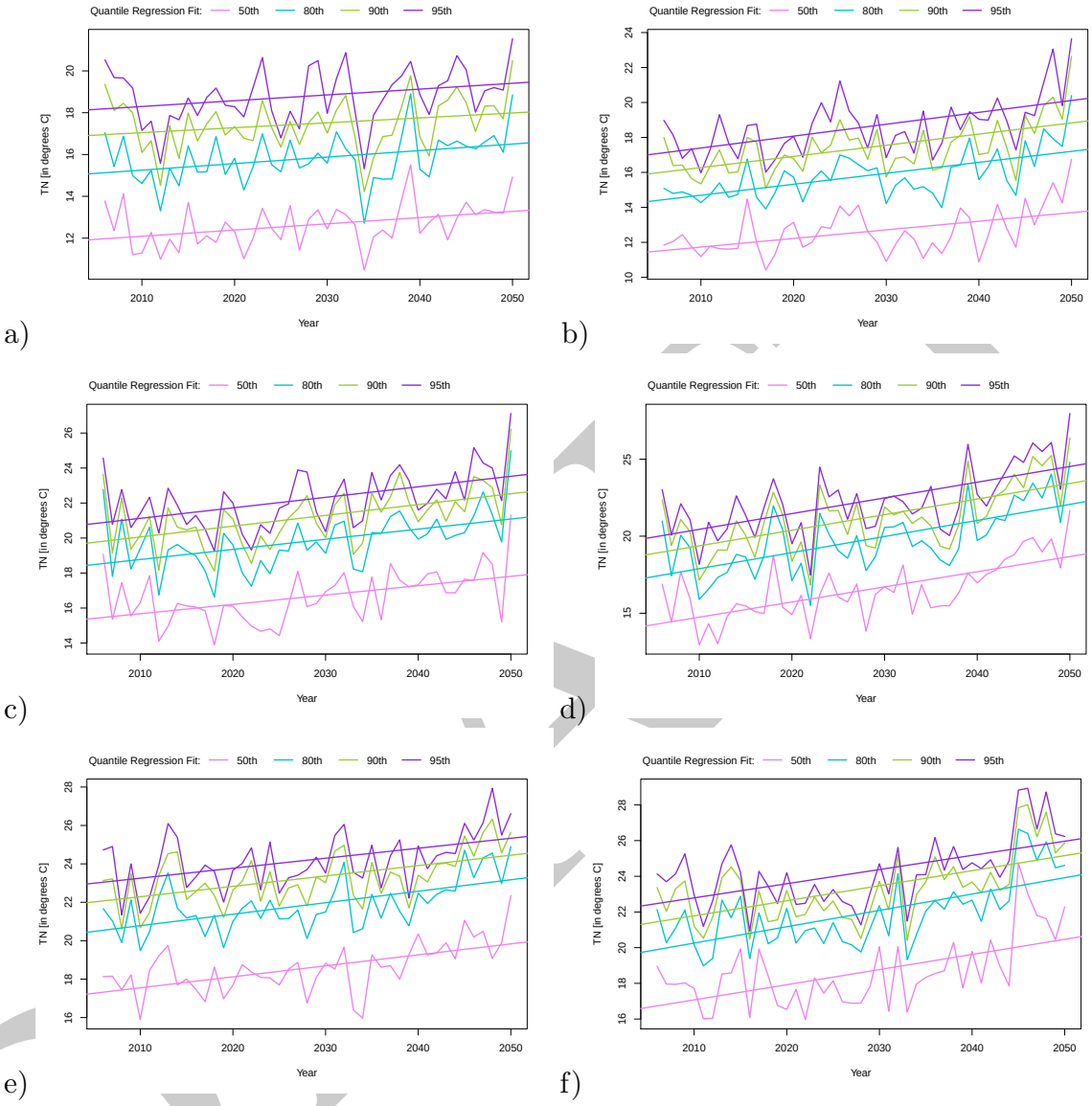

FIG. 5. Quantile regression trends of seasonal minimum temperatures TN for scenarios RCP2.6 and RCP8.5 of a) Stuttgart RACMO RCP2.6 b) RCP8.5, c) Montpellier RACMO RCP2.6, d) RCP8.5 and e) Seville REMO2009 RCP2.6 and f) RCP8.5 for different percentiles in 2006-2050. For the quantile regressions bias-corrected RCM temperatures have been used.

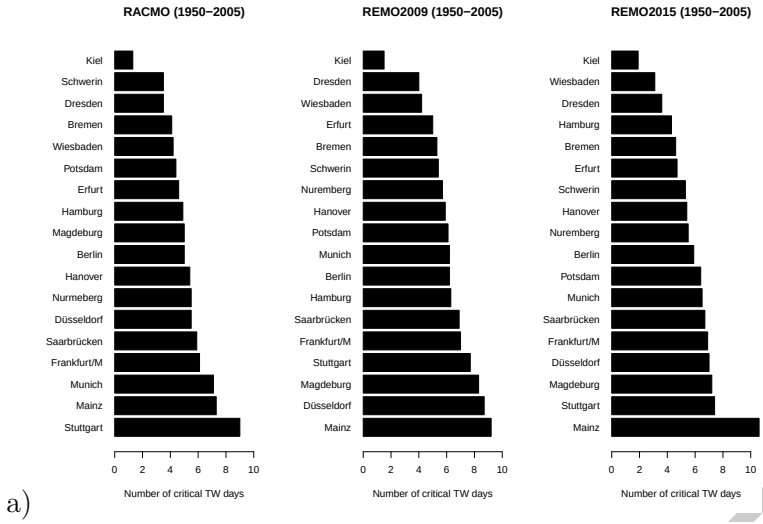

a)

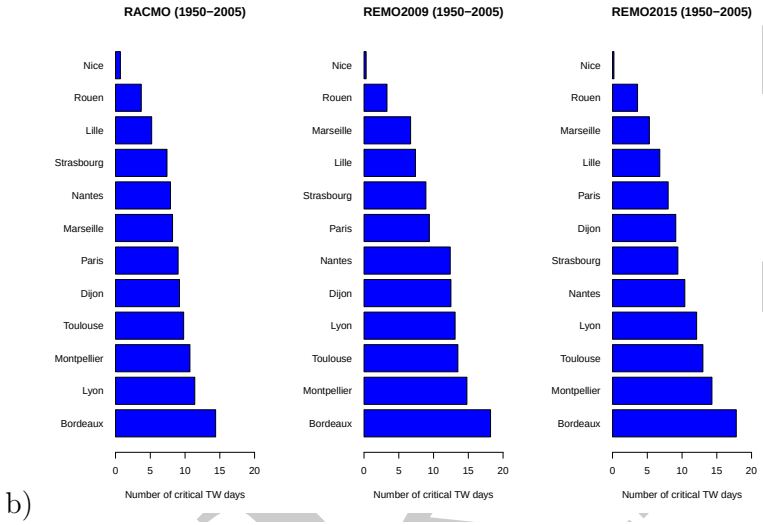

b)

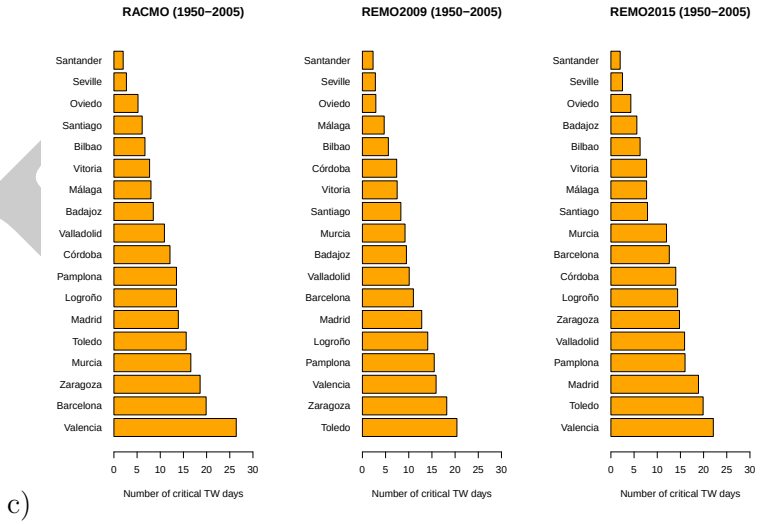

c)

988 FIG. 6. Increase in the number of critical TW days in a) German, b) French and c) Spanish cities
989 over the period 1950-2005.

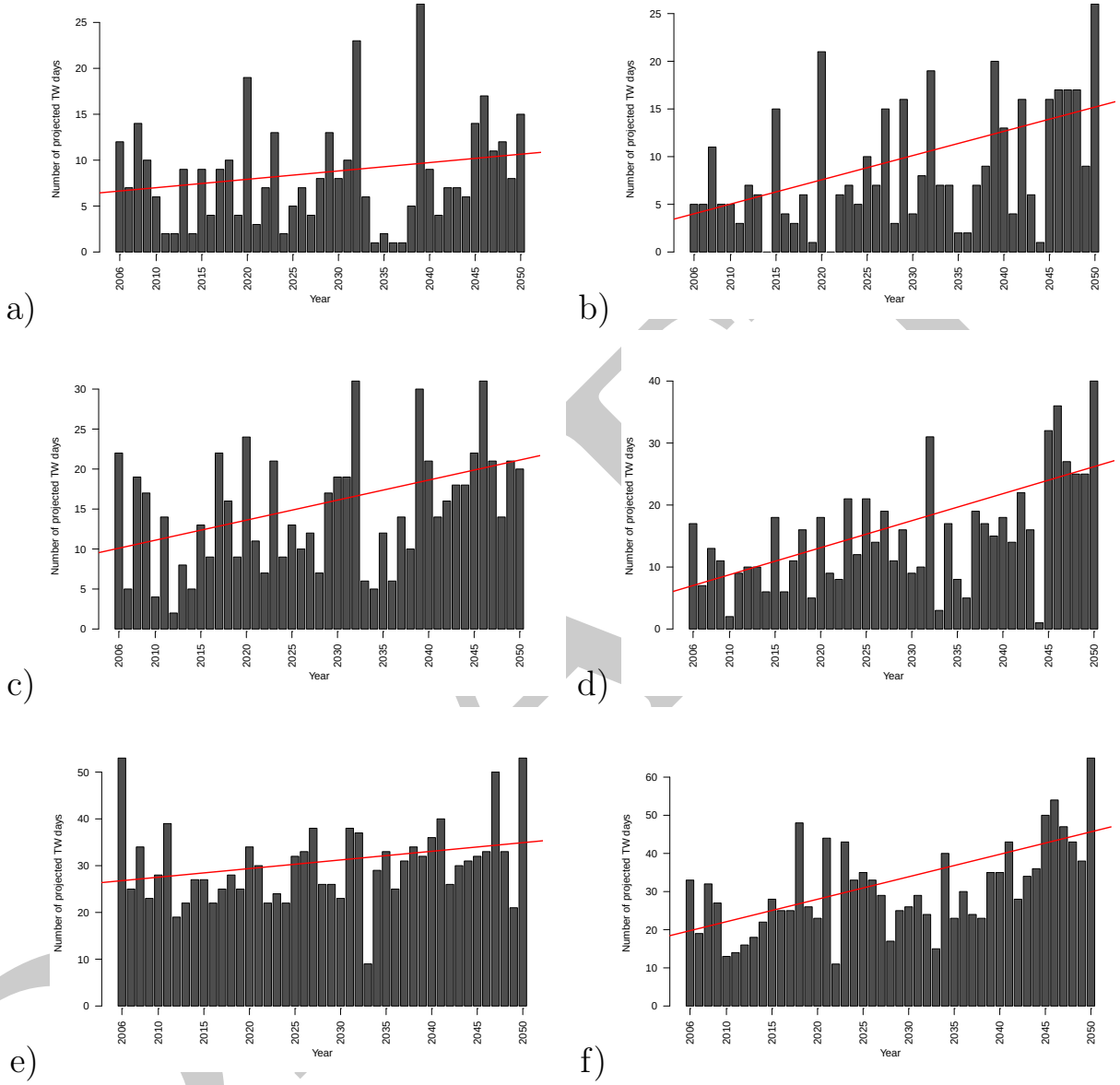

990 FIG. 7. Seasonal wet-bulb temperatures TW for scenarios RCP2.6 and RCP8.5 with linear regres-
991 sion trend (red line) of a) Saarbrücken RACMO RCP2.6 b) RCP8.5, c) Bordeaux RACMO RCP2.6, d)
992 RCP8.5 and e) Zaragoza REMO2009 RCP2.6 and f) RCP8.5 for different percentiles in 2006-2050.

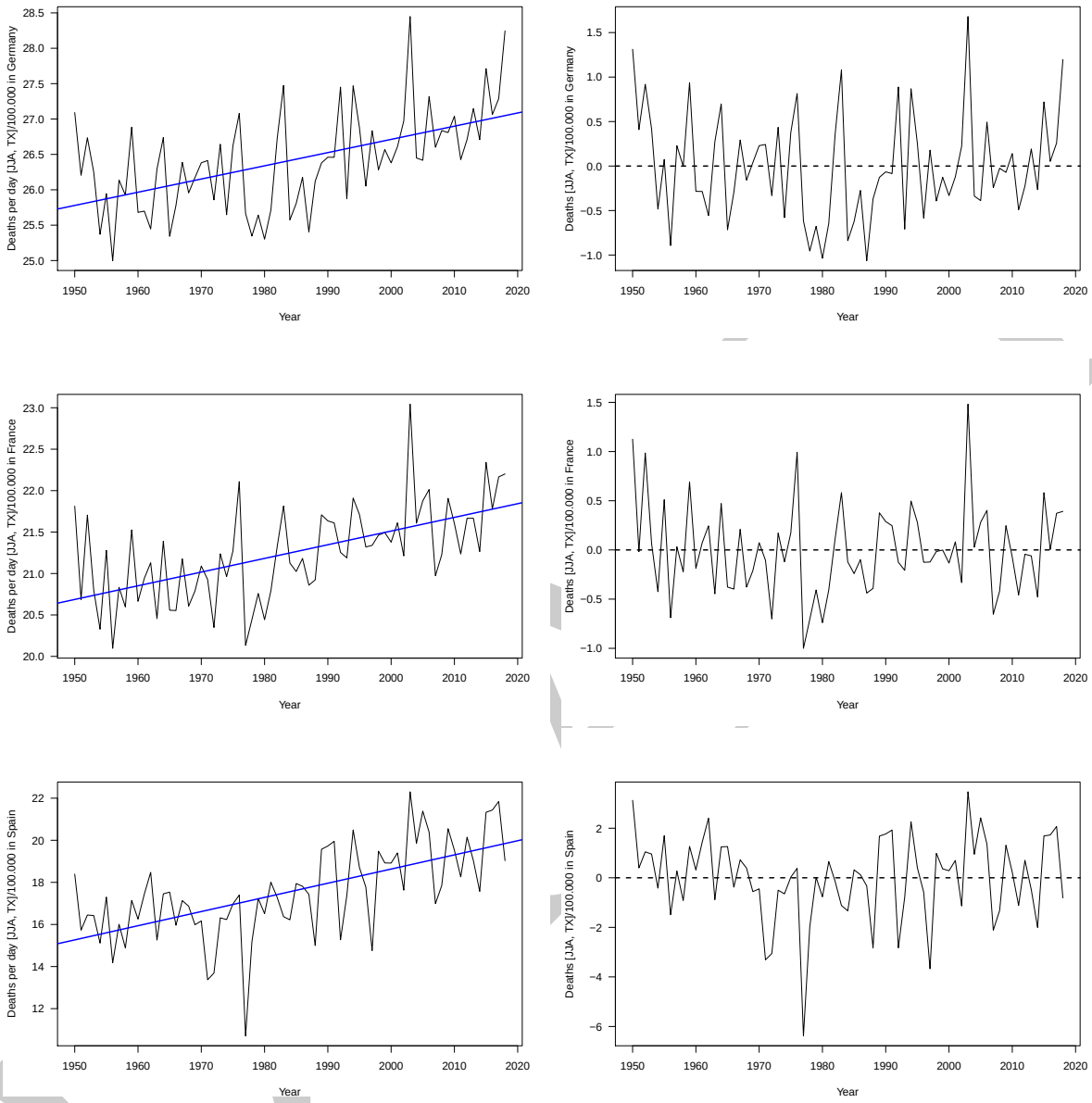

993 FIG. 8. Excess heat deaths per 100.000 residents with regression line (left) and normalized
994 (detrended) excess heat heat deaths (right) in Germany, France and Spain in 1950-2018.

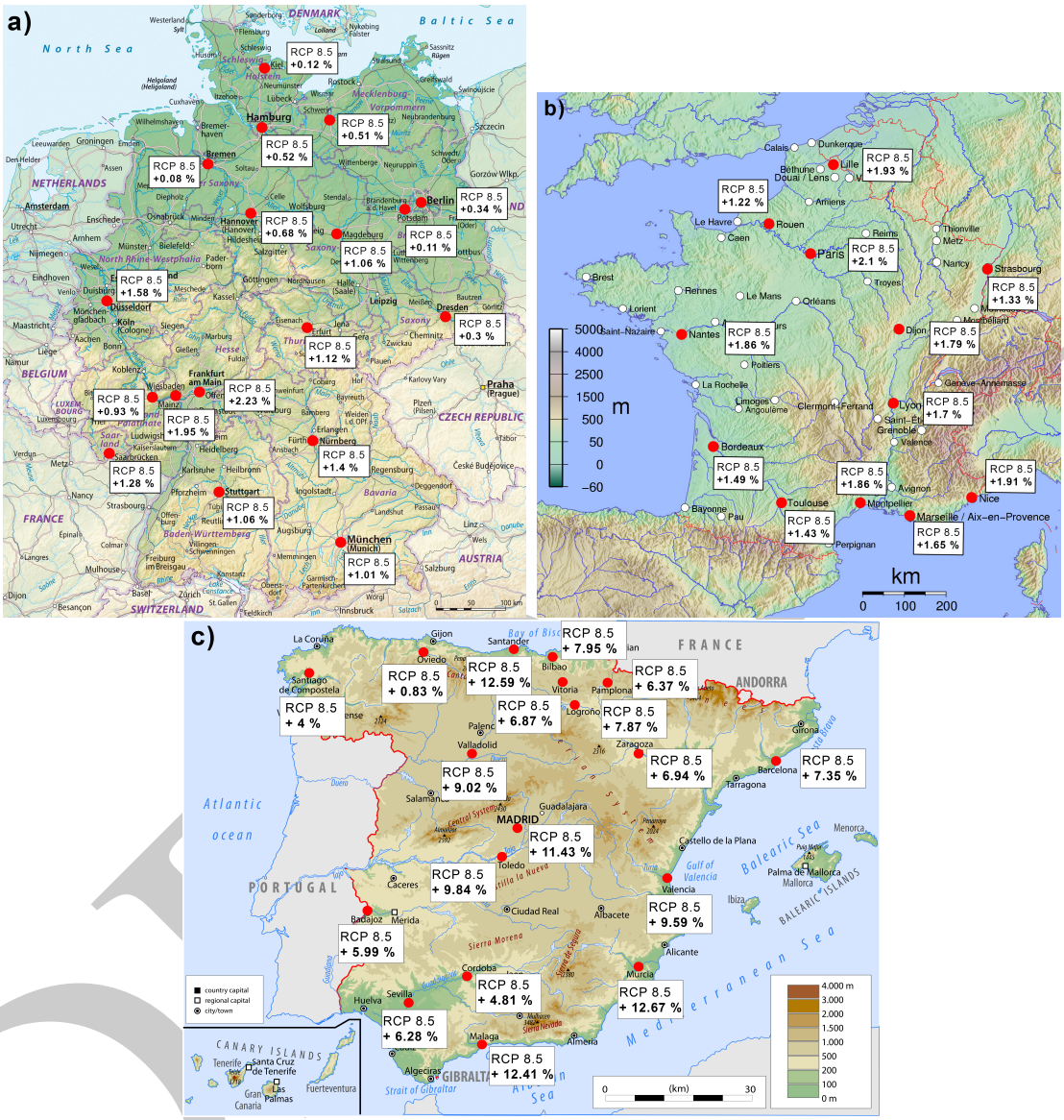

995 FIG. 9. Trend slope of heat mortality for future climate projections [in %/decade] derived from
996 daily TX observations and excess deaths in RCP8.5 for cities in a) Germany, b) France and c) Spain
997 in 2019-2050 (Map sources: World of Maps (2019), My Geo Info (2019), World Atlas (2019)).